



LANE KEEPING CONTROL FOR SELF-DRIVING VEHICLES

KIVANÇ SARAÇOĞLU

JANUARY 2018

LANE KEEPING CONTROL FOR SELF-DRIVING VEHICLES

**A THESIS SUBMITTED TO
THE GRADUATE SCHOOL OF NATURAL AND APPLIED
SCIENCES OF
ÇANKAYA UNIVERSITY**

**BY
KIVANÇ SARAÇOĞLU**

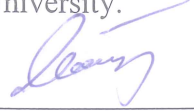
**IN PARTIAL FULFILLMENT OF THE REQUIREMENTS FOR THE
DEGREE OF
MASTER OF SCIENCE
IN
THE DEPARTMENT OF
ELECTRONIC-COMMUNICATION ENGINEERING**

JANUARY 2018

Title of the Thesis: **Lane Keeping Control for Self-Driving Vehicles**

Submitted by **Kıvanç SARAÇOĞLU**

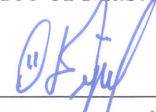
Approval of the Graduate School of Natural and Applied Sciences, Çankaya University.



Prof. Dr. Can ÇOĞUN

Director

I certify that this thesis satisfies all the requirements as a thesis for the degree of Master of Science.



Yrd. Doç. Dr. Özgür ERGÜL
Head of Department V.

This is to certify that we have read this thesis and that in our opinion it is fully adequate, in scope and quality, as a thesis for the degree of Master of Science.



Assoc. Dr. Klaus Werner Schmidt
Supervisor

Examination Date: 19.01.2018

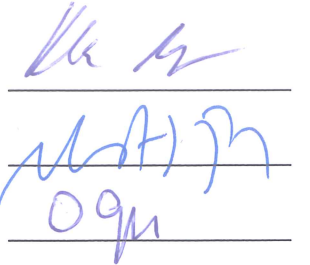
Examining Committee Members

Assoc. Prof. Dr. Klaus Werner (METU)

SCHMIDT

Assoc. Prof. Dr. Mustafa DOĞAN (ITÜ)

Assoc. Prof. Dr. Orhan GAZİ (Çankaya Univ)



STATEMENT OF NON-PLAGIARISM PAGE

I hereby declare that all information in this document has been obtained and presented in accordance with academic rules and ethical conduct. I also declare that, as required by these rules and conduct, I have fully cited and referenced all material and results that are not original to this work.

Name, Last Name : Kivanç Saraçođlu

Signature

:



Date

:

19/01/2018

ABSTRACT

LANE KEEPING CONTROL FOR SELF-DRIVING VEHICLES

SARAÇOĞLU, Kivanç

MSc. Department of Electronic and Communication Engineering

Supervisor: Assoc. Prof. Dr. Klaus Werner SCHMIDT

19 January 2018, 69 pages

Intelligent Transportation Systems including Lane Keeping Systems (LKS) aim at providing comfort to drivers, preventing congestion, decreasing gas and CO₂ emissions and the number of traffic accidents. LKSs will be widely employed in the automobile industry in the near future as an essential part of modern vehicles including cars, buses and trucks.

When realizing a LKS, it is necessary to decide about the required signal measurements and to implement control algorithms that are suitable for different vehicle speeds, road curvatures and can be adapted to different types of vehicles such as passenger vehicles, buses and trucks.

The main aim of this thesis is to evaluate and compare different lane keeping algorithms. These lane keeping algorithms are applied to a vehicle model, whose longitudinal motion is decoupled from the lateral motion. Four lane keeping control algorithms are investigated. The first two control algorithms measure the yaw rate and the displacement error at a pre-view distance to compute the necessary rate of change of the steering angle for following a road. The first control algorithm uses a linear controller transfer function, whereas the second control algorithm uses sliding mode control. The third control algorithm also measures the yaw rate and the displacement error at a pre-view distance but directly computes the required steering angle for lane keeping. The fourth control algorithm measures the yaw rate,

the heading error and the displacement of the center of gravity (COG). These algorithms are evaluated using simulation experiments with given displacement errors and road profiles.

The main outcomes of the thesis are as follows. As the first contribution, the thesis shows that the measurement of the displacement error at a pre-view distance increases the robustness of lane keeping control algorithms. On the downside, since the displacement error at the pre-view distance is controlled, the displacement error at the COG can become large at high velocities. As the second contribution, the thesis concludes that it is beneficial to combine measurements of the yaw rate, the displacement errors at the preview-distance and the COG as well as a prediction of the road curvature to obtain an efficient control algorithm. Such control algorithm is proposed in the thesis and its superior performance is shown by simulation experiments.

Keywords: Intelligent transportation systems, lane keeping, longitudinal motion, lateral motion, linear vehicle model, nonlinear vehicle model.

ÖZ

SARAÇOĞLU, Kıvanç

Y.Lisans., Elektronik ve Haberleşme Mühendisliği Anabilim Dalı

Tez Yöneticisi: Doç. Dr. Klaus Werner SCHMIDT

19 Ocak 2018, 69 sayfa

Akıllı ulaşım sistemlerinden birisi olan Şerit Koruma Sistemi (LKS) sürücülerin konforunu artırırken trafikteki yığılmayı ve trafik kazalarını azaltırken , zararlı gaz ve CO_2 emisyonunu da düşürmektedir.

Otomobil endüstrisinin yakın gelecekte Şerit Koruma Sistemlerini otomobil, otobüs ve kamyonlar dahil araçların ayrılmaz bir parçası olarak kullanacağı şimdiden öngörülebilir.

Bir Şerit Kontrol Sistemini doğru çalışabilmesi için, binek araçları, otobüsler ve kamyonlar dahil değişik araçlar için, farklı hızlara ve virajlara uygun olan sinyal ölçümlerini yapabilmesi ve gerekli kontrol algoritmalarını uygulayabilmesi gerekmektedir.

Bu tezin temel amacı farklı şerit koruma algoritmalarını değerlendirmek ve birbirleriyle karşılaştırmaktır. Bu şerit koruma algoritmaları, uzunlamasına hareketi yanal harekete aykırı olan bir taşıt modeline uygulanarak araştırılmıştır. Dört şeridi koruma kontrol algoritmaları incelenmiştir. İlk iki kontrol algoritması bir şeridi takip ederken sürüş açısındaki değişiklikleri hesaplayabilmek için gerekli olan dönüş hızını ve yer değiştirme hatasını ölçmektedir. Birinci kontrol algoritması doğrusal kontrolün transfer fonksiyonunu kullanırken, ikinci kontrol algoritması kayma modu kontrolünü kullanmaktadır. Üçüncü kontrol algoritması belirlenmiş bir mesafedeki dönüş hızını ve yer değiştirme hatasını ölçerken , doğrudan şeridi korumak için gerekli olan sürüş açısını da hesaplamaktadır. Dördüncü kontrol

algoritması , dönüş hızını, istikamet hatasını ve ağırlık merkezindeki yer değişikliğini (COG) ölçmektedir. Bu algoritmalar verilen yer değiştirme hataları ve yol profillerinde simülasyon deneyleri yapılarak değerlendirilmiştir.

Tezin başlıca sonuçları şunlardır: İlk katkı olarak, tez, bir ön görüş mesafesinde yer değiştirme hatasının ölçülmesinin, şerit tutma kontrol algoritmalarının sağlamlığını arttırdığını göstermektedir. Olumsuz yönü ise ön izleme mesafesindeki yer değiştirme hataları kontrol edildiğinde, yüksek hızlarda ağırlık merkezindeki yer değiştirme hataları daha büyük olduğu bulunmuştur.

Tezden elde edilen ikinci sonuç ise, etkili bir kontrol algoritması elde edilebilmesi için dönüş hızı , ön izleme mesafesindeki yer değiştirme hatası ve ağırlık merkezindeki yer değiştirmenin birlikte ölçülmesi ve yol kavisinin tahmin edilmesi daha yararlı olmaktadır. Tezde benzeri bir kontrol algoritması önerilmiş ve bu sistemin üstün başarısı simülasyon testleriyle de gösterilmiştir.

Anahtar Kelimeler: Akıllı iletim sistemleri , Şerit koruma, boylamasına hareket, yanlamasına hareket, doğrusal araç modeli, doğrusal olmayan araç modeli

ACKNOWLEDGEMENTS

I would like to express my special thanks of gratitude to Assoc.Prof. Klaus Werner Schmidt for his extraordinary supervision, very special guidance, suggestions, and encouragement through the development of this thesis. He gave me the golden opportunity to do this wonderful thesis which also helped me in doing a lot of research and I come to know about so many new things I am really thankful to him.

It is a pleasure for me to express my special thanks to my family for their valuable support during whole my life.

Finally, I would like to thank TÜBİTAK. Part of the work was done in the scope of the TÜBİTAK project with the number 115E372.

TABLE OF CONTENTS

STATEMENT OF NON PLAGIARISM.....	iii
ABSTRACT.....	iv
ÖZ	vi
ACKNOWLEDGMENT.....	viii
TABLE OF CONTENTS.....	ix
LIST OF FIGURES.....	xi
LIST OF TABLES.....	xiv
LIST OF ABBREVIATIONS.....	xv

CHAPTERS:

1. INTRODUCTION.....	1
2. BACKGROUND.....	5
2.1 Nonlinear Vehicle Model.....	5
2.2 Decoupled Vehicle Model.....	7
2.3 Linearized Model.....	8
2.4 Distance from Road and Heading Error Measurement.....	8
2.5 Simulations, comparison of decoupled vehicle model and linearized vehicle model	11
2.5.1 Vehicle Parameters	11
2.5.2 Motion on Straight Road.....	11
2.5.3 Straight Motion and Curved Road.....	16
3. LANE KEEPING ANALYSIS.....	20
3.1 Test Setup and General Remarks.....	20
3.2 Linear Controller According to [52].....	21

3.2.1 Controller Structure.....	22
3.2.2 Evaluation for the Bus Parameters.....	22
3.2.3 Evaluation for the Car Parameters.....	29
3.3 Sliding Mode Controller.....	30
3.3.1 Description.....	30
3.3.2 Evaluation for Bus Parameters.....	32
3.3.3 Evaluation for Passenger Car Parameters.....	38
3.4 Nested PID Control.....	40
3.4.1 Description.....	40
3.4.2 Evaluation for the Bus Parameters	41
3.4.3 Evaluation for Car Parameters.....	48
3.5 Empirical Controller	50
3.5.1 Description.....	50
3.5.2 Evaluation for the Bus Parameters	51
3.5.3 Evaluation for Car Parameters	54
3.6 Suggested Controllers.....	55
3.7 Comparison of all Controllers.....	58
4. CONCLUSIONS	62
REFERENCES.....	63
CURRICULUM VITAE.....	69

LIST OF FIGURES

Figure 1.1:	Lane keeping System.....	2
Figure 2.1:	Dynamic Bicycle Model.....	5
Figure 2.2:	Vehicle on the road.....	8
Figure 2.3:	Distance Computation.....	10
Figure 2.4:	Periodic change of the steering angle for the bus up to 5°	12
Figure 2.5:	Periodic change of the steering angle for the bus up to 2°	13
Figure 2.6:	Periodic change of the steering angle for the bus up to 20°	14
Figure 2.7:	Left and right turns of the bus with a steering angle up to 2.5°	15
Figure 2.8:	Left and right turns of the bus with a steering angle up to 5°	16
Figure 2.9:	Left and right turns of the road with a frequency of 0.5 rad/sec.....	17
Figure 2.10:	Left and right turns of the road with a frequency of 2 rad/sec.....	18
Figure 2.11:	Right and left turn of the road.....	19
Figure 3.1:	Road approach from initial error.....	21
Figure 3.2:	Test road with different curvatures.....	22
Figure 3.3:	Response for an initial displacement error of 1 m (bus parameters).....	24
Figure 3.4:	Following the test road at $v = 10$ m/s with $l_s = 12$ m (bus parameters).....	25
Figure 3.5:	Following the test road at $v = 20$ m/s with $l_s = 12$ m (bus parameters).....	25
Figure 3.6:	Following the test road at $v = 30$ m/s with $l_s = 12$ m (bus parameters).....	26
Figure 3.7:	Following the test road at $v = 10$ m/s with $l_s = 6$ m (bus parameters).....	27
Figure 3.8:	Following the test road at $v = 20$ m/s with $l_s = 6$ m (bus parameters).....	28
Figure 3.9:	Following the test road at $v = 30$ m/s with $l_s = 6$ m (bus parameters).....	28
Figure 3.10:	Response for an initial displacement error of 1 m	

	(car parameters).....	29
Figure 3.11:	Following the test road at $v = 10$ m/s with $l_s = 6$ m (car parameters).....	30
Figure 3.12:	Sliding mode control loop.....	31
Figure 3.13:	Response for an initial displacement error of 1 m (bus parameters).....	33
Figure 3.14:	Sliding mode controller on the test road $v=10$ m/s and $l_s = 12$ m (bus parameters).....	34
Figure 3.15:	Sliding mode controller on the test road $v=20$ m/s and $l_s = 12$ m (bus parameters).....	35
Figure 3.16:	Sliding mode controller on the test road $v=30$ m/s and $l_s = 12$ m (bus parameters).....	36
Figure 3.17:	Sliding mode controller on the test road $v=10$ m/s and $l_s = 6$ m (bus parameters).....	37
Figure 3.18:	Sliding mode controller on the test road $v=20$ m/s and $l_s = 6$ m (bus parameters).....	38
Figure 3.19:	Sliding Mode Response for an initial displacement error of 1 m (car parameters)	39
Figure 3.20:	Sliding mode controller on the test road $v=20$ m/s and $l_s = 12$ m (car parameters).....	40
Figure 3.21:	Nested feedback loop.....	41
Figure 3.22:	Nested PID: Response for an initial displacement error of 1 m (bus parameters).....	42
Figure 3.23:	Nested PID control on the test road: $V = 10$ and $l_s = 12$ m (bus parameters)	43
Figure 3.24:	Nested PID control on the test road : $V = 20$ and $l_s = 12$ (bus parameters).....	44
Figure 3.25:	Nested PID control on the test road : $V = 30$ and $l_s = 12$ (bus parameters).....	45
Figure 3.26:	Nested PID control on the test road : $V = 10$ and $l_s = 6$ (bus parameters).....	46
Figure 3.27:	Nested PID control on the test road : $V = 20$ and $l_s = 6$ (bus parameters).....	47
Figure 3.28:	Nested PID control on the test road : $V = 30$ and $l_s = 6$ (bus parameters).....	48
Figure 3.29:	Nested PID : Response for an initial displacement error of 1 m (car parameters).....	49
Figure 3.30:	Nested PID control on the test road : $V = 30$ and $l_s = 6$ (car parameters)....	50

Figure 3.31: Empirical control: Initial displacement error of 1 m (bus parameters).....	51
Figure 3.32: Empirical control on the test road: $v=10$ m/s (bus parameters).....	52
Figure 3.33: Empirical control on the test road: $v=20$ m/s (bus parameters).....	53
Figure 3.34: Empirical control on the test road: $v=30$ m/s (bus parameters).....	54
Figure 3.35: Empirical control on the test road: $v=20$ m/s (car parameters).....	55
Figure 3.36: Proposed Control: Initial displacement error of 1 m (bus parameters).....	56
Figure 3.37: Proposed control on the test road: $v=10$ m/s (bus parameters).....	57
Figure 3.38: Proposed control on the test road: $v=20$ m/s (bus parameters).....	57
Figure 3.39: Proposed control on the test road: $v=30$ m/s (bus parameters).....	58
Figure 3.40: Controller Comparison: Initial displacement error of 1 m (bus parameters).....	59
Figure 3.41: Controller Comparison on the test road: $v=10$ m/s (bus parameters).....	60
Figure 3.42: Controller Comparison on the test road: $v=20$ m/s (bus parameters).....	60
Figure 3.43: Controller Comparison on the test road: $v=30$ m/s (bus parameters).....	61

LIST OF TABLES

Table 2.1:	Vehicle Parameters.....	11
-------------------	-------------------------	----



LIST OF ABBREVIATIONS

IVS	Intelligent Vehicle Systems
AHS	Automated Highway Systems
COG	Center of Gravity.
X	Longitudinal Position.
Y	Lateral Position.
V	Vehicle Speed
δ	Steering Angle.
$\Delta\psi$	Yaw Angle.
M	Vehicle Mass.
J	Moment of Inertia.
β	Slip Angle.
l_s	Look-Ahead Distance.
\dot{v}	Vehicle Acceleration
P	<i>Road Curvature</i>
R	<i>The Road Radius.</i>
P_s	Starting Point.
P	The Distance of Point From Road.
L	The length of Line Segment.
F_{lf}	Longitudinal force at the front wheel in the wheel direction.
F_{lr}	Longitudinal force at the rear wheel in wheel direction is zero if rolling is assumed.
F_{cf}	Lateral (cornering) force at the front wheel perpendicular to the the wheel direction.
F_{cr}	Lateral force at the rear wheel perpendicular to the wheel direction.
α_f	Tire Slip (front wheel).
α_r	Tire Slip (rear wheel).
F_{xf}	Longitudinal Forces (front wheel).
F_{xr}	Longitudinal Forces (rear wheel).
F_{yf}	Lateral Force (front wheel).
F_{yr}	Lateral Force (rear wheel)

CHAPTER 1

INTRODUCTION

Driver error is the reason in more than 90% of all traffic accidents [9]. In a survey in the United States of America in 2012, it is found that 21 % of the traffic accidents were due to fatigue of the drivers, who were driving extended period of time in the highways [5]. For decreasing the driving load of the drivers, for increasing their performance and for safety and prevention of traffic accidents user-friendly cars are developed with new systems [6],[7],[8]. [10], [11], [12]. These include vision-based driver assistance systems such as blind spot detection system (BDS), lane departure warning system (LDWS), forward collision warning system (FCWS) and lane keeping system (LKP) [1,2,3]. In particular, lane keeping is one of the essential parts of an intelligent vehicle system to automate the lateral vehicle motion [4].

Lane keeping (LK) system is one of the most important parts of a self-driving vehicle. The task is to hold the vehicle in the center of the lane, which is commonly achieved by the help of various sensors, a front-view camera system and a steering actuator [13]. The basic components of a lane keeping system are shown in Fig. 1.1. The front-view camera system takes the images of the road, detects the lane markings and identifies the position and orientation of the vehicle with respect to the lane. Then, a control algorithm computes the necessary steering angle to keep the vehicle on the lane or move the vehicle to the road center. Full automation of a lane keeping system removes the need for lateral vehicle control by a driver. Therefore the human factors which may cause the traffic accidents are prevented [14,15,16].

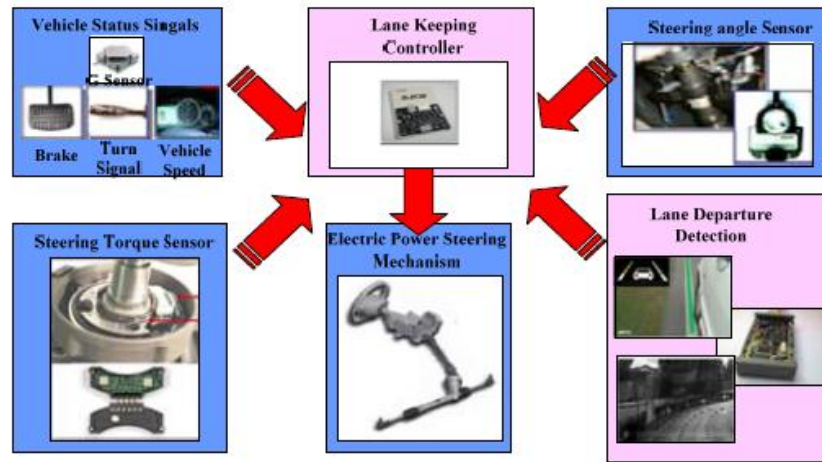


Figure 1.1: Lane keeping system

A considerable amount of research was performed on the topic of lane keeping. Some of them are related to steering, braking and throttling of a single or group of vehicles. Mammar [17, 18] developed different control algorithms for lane keeping based on state feedback control and fuzzy control. Hatipoğlu and co-workers [19, 20] designed an H_∞ controller for automatic steering of vehicles in order to keep the vehicle's center of gravity close to the center of the lane. Liu, Hu and Hsu [13] developed a lane keeping control system for vehicle which is based on the structure of electric power steering based on a vision-based lane departure detection unit. Raksincharoensak and co-workers [21] used model matching control for a four wheel steering system. Raharijaona, Duc and Mammar [22] studied the H_∞ design of for the lateral driving assistance with lane keeping and yaw dynamics enhancement. You and Jeong [23] worked on a two- degree-of freedom based H_∞ loop-shaping control scheme for lane keeping and changing manoeuvres. Zambou and co-workers [24] proposed MPC and Robust loop shaping control design to improve the automatic steering assistance systems of vehicles having a low velocity range. Jung and Kelber [25] described a technique for the detection of lane departur. For tracking, a linear- parabolic model is tested while a linear model is used to get robust information. In a study done by Wang and co-workers [26], a new lane keeping control scheme including tractor front wheel steering, tractor rear wheel steering, and trailer wheel steering is developed. Cerone and co-workers [28] investigated the problem of combining automatic lane keeping and driver's steering for either obstacle avoidance or lane change maneuvers for any desired maneuvers by using a

closed loop control strategy.

Zhang and Ren [30] studied the problem of lane keeping in the presence of parametric uncertainty. Wang, Lin and Chen [32] use fuzzy methods for lane detection and calculate angle relations for lane departure warning. Zhao, Lefranc and El Kamel [33] proposed a multi-model fuzzy controller for both lane keeping and lane changing. Ping and Swee [35] established a 9-Degree of freedom vehicle model together with a closed-loop driver model for automatic steering control. Doi and co-workers [36] develop a steering-assist control method based on estimated virtual road boundary information. Mashadi and co-workers [37] provided a controller for tracking the driver intended path of an integrated driver/vehicle system. Rucco, Notarstefano and Hauser [38] presented optimal control-based strategies to explore the dynamic capabilities of a single-track car model including tire models and longitudinal load transfer. Chen, Luan and Lee [39] worked on a lane keeping system which is using adaptive model predictive control. Williams [40] improved the classic two degree of freedom yaw-plane or bicycle vehicle model with two additional states in representing lane-keeping behavior. Son and co-workers [41] studied a new approach for a robust multirate lane-keeping control scheme having predictive virtual lanes. Lei [42] described a sliding mode lane keeping method with hybrid information of position and angular velocity which is based on the simplified lateral dynamics model of automatic driving vehicle and its mass movement equation.

Martinez-Garcia, Zhang and Gordon [43] proposed a new methodology for modelling human lane keeping control by defining a unique concept of elementary steering. Lei, and co-workers [44] proposed a simplified linear lateral dynamic model about lane keeping for automatic driving of vehicles. Kim, Son and Chung [45] presented a torque-overlay-based robust steering wheel angle (SWA) control method of electrical power steering (EPS) for lane-keeping.

In this thesis, lane keeping is studied in the context of self-driving vehicles. In this case, it is important that both the longitudinal and the lateral vehicle motion can be controlled. In particular, it should be possible adjust the vehicle velocity independent of the lateral vehicle motion. To this end, the first contribution of the thesis is to use a new decoupling strategy that removes the effect of the lateral vehicle motion on the

longitudinal vehicle motion. The resulting vehicle model is different from the vehicle models used for existing lane keeping systems. In addition, it is necessary to evaluate the performance of lane keeping systems. This thesis is based on four lane keeping algorithms that are prominent in the existing literature. A linear control algorithm and a sliding mode controller are adopted from [52]. In addition the method by Marini, Scalzi and Netto [51], which propose a nested PID steering control is considered. Finally, the empirical control algorithm in [56] is taken into account. As the second contribution, the thesis implements the cited control algorithms in MATLAB/Simulink and performs a comprehensive comparative simulation study. It is shown that most of the existing algorithms have a particular disadvantage that was not identified in the literature before. Since the algorithms control the displacement error of the vehicle at a given pre-view distance, it turns out that the actual vehicle displacement can assume unnecessarily large values on curved roads. Only one algorithm directly controls the vehicle displacement. However, this algorithm has the disadvantage of large oscillations around the road center which are undesired. As a remedy, the third contribution of the thesis is a new lane keeping control method that combines measurements of the actual vehicle displacement (for precision) and the vehicle displacement at a pre-view distance (for robustness). The comparative simulation study in the thesis shows that the proposed method has superior performance compared to the existing methods.

The thesis is organized as follows. Chapter 2 give background information and introduced the relevant linear and nonlinear vehicle models. Chapter 3 first describes the existing control algorithms and evaluates their performance in different driving scenarios. Then, a new lane keeping algorithms I proposed and compared to the existing algorithms. Conclusions are given in Chapter 4.

CHAPTER 2

BACKGROUND

The background information for lane keeping control in this thesis is given with detail in this chapter. First, the nonlinear vehicle model is introduced in Section 2.1. A decoupling strategy from the recent work is explained in Section 2.2. Section 2.3 linearizes the nonlinear vehicle model for later analysis. Section 2.4 extends the models by the road geometry.

2.1 Nonlinear Vehicle Model

The studies performed in the thesis is based on the dynamic bicycle model [47] [48] [49] [50] model as shown in Fig. 2.1. The model [54] is developed by combining the two front wheels into one wheel in the centerline of the vehicle.

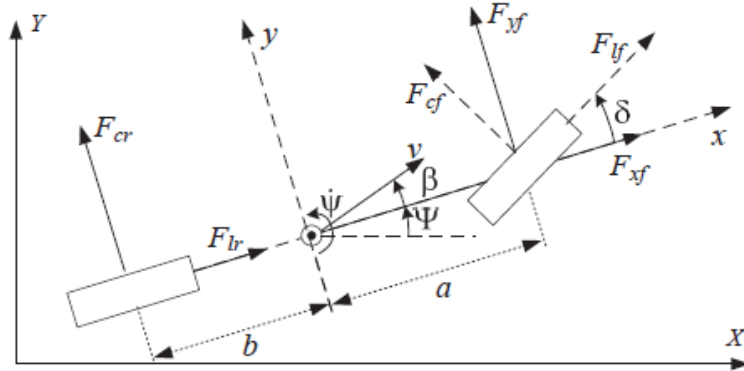


Figure 2.1: Dynamic Bicycle Model

In the model, there are some coordinate frames. In order to describe the inertial frame, the signals X , Y (position) and Ψ (angle) are used. On the other hand, the body frame which is fixed to the vehicle body is connected to the center of gravity (COG) with signals x , y , and ψ (angle). Beside those, the side-slip angle β is defined as $\beta = \tan^{-1} \left(\frac{\dot{x}}{\dot{y}} \right)$. The relation between the inertial coordinate and body coordinates [47] [48]

[49] is given by

$$\dot{X} = \dot{x} \cos (\Psi) - \dot{y} \sin (\Psi) \quad (2.1)$$

$$\dot{Y} = \dot{x} \sin (\Psi) + \dot{y} \cos (\Psi) \quad (2.2)$$

$$\dot{\Psi} = \dot{\psi} \quad \dots \quad (2.3)$$

Steering of a vehicle is commonly performed by the adjustment of the steering angle δ of the front wheel. The forces acting on the vehicle can be written in the wheel direction or in the body coordinates. When a vehicle with front-wheel drive is considered, the following forces act on the wheels in the wheel direction (see also Fig. 2.1).

F_{xf} : longitudinal force acting on the front wheel in the wheel direction

F_{cf} : lateral (cornering) force acting on the front wheel perpendicular to the wheel direction

F_{lr} : longitudinal force acting on the rear wheel in wheel direction is zero if rolling is assumed

F_{cr} : lateral force acting on the rear wheel perpendicular to the wheel direction

The dynamic equations in the body frame [50] are as follows

$$\ddot{x} = \dot{y} \dot{\psi} + \frac{F_{xf} + F_{xr}}{m} \quad (2.4)$$

$$\ddot{y} = -\dot{x} \dot{\psi} + \frac{F_{yf} + F_{yr}}{m} \quad (2.5)$$

$$\ddot{\psi} = \frac{aF_{yf} - bF_{yr}}{J} \quad (2.6)$$

where m is the vehicle mass, J is the moment of inertia and l_f, l_r are the distances between the wheels and the COG [48]. The longitudinal forces F_{xf}, F_{xr} and the lateral forces F_{yf}, F_{yr} at the front and rear tires depend on the respective forces in the wheel direction named as F_{lf}, F_{cf}, F_{lr} and F_{cr} [49]. These forces are calculated by using (2.7) to (2.10):

$$F_{xf} = F_{lf} \cos(\delta) - F_{cf} \sin(\delta) \text{ (front wheel, x-direction)} \quad (2.7)$$

$$F_{yf} = F_{lf} \sin(\delta) + F_{cf} \cos(\delta) \text{ (front wheel, y-direction)} \quad (2.8)$$

$$F_{xr} = F_{lr} = 0 \text{ (rear wheel, x-direction)} \quad (2.9)$$

$$F_{yr} = F_{cr} \text{ (rear wheel, y-direction)} \quad (2.10)$$

F_{lf} is the traction force coming from the engine and $F_{lr} = 0$ if actuation is used at the front tires. The lateral tire slip angles α_f (front) and α_r (rear) of the respective tire are used to find the forces F_{cf} and F_{cr} with tire stiffness constants c_f and c_r .

$$\alpha_f = \tan^{-1}\left(\frac{\dot{y} + a \dot{\psi}}{\dot{x}}\right) - \delta \quad (2.11)$$

$$\alpha_r = \tan^{-1}\left(\frac{\dot{y} - b \dot{\psi}}{\dot{x}}\right) \quad (2.12)$$

$$F_{cf} = -\alpha_f \cdot c_f \quad (2.13)$$

$$F_{cr} = -\alpha_r \cdot c_r \quad (2.14)$$

In addition, an alternative method that is used the first time-derivatives of the position coordinates derived based on the side-slip angle β can be utilized for the dynamic vehicle model with the velocity [46] $v = \sqrt{\dot{x}^2 + \dot{y}^2}$. By replacing (2.4) and (2.6), the following equations can be found and written as:

$$\dot{\beta} = \frac{F_{cr} \cdot \cos(\beta) + F_{cf} \cdot \cos(\beta - \delta) - F_{lf} \cdot \sin(\beta - \delta)}{mv} - \dot{\psi} \quad (2.15)$$

$$\ddot{\psi} = \dot{r} = \frac{(F_{lf} \sin(\delta) + F_{cf} \cos(\delta)) l_f - F_{cr} l_r}{J} \quad (2.16)$$

In addition, the arc length can be introduced as the traveled distance of the vehicle. It is computed as $\dot{q} = v$. Hence, its derivative (which is the vehicle acceleration) is

$$\ddot{q} = \dot{v} = \cos(\beta) \cdot \ddot{x} + \sin(\beta) \cdot \ddot{y} = \frac{F_{cr} \sin(\beta) + F_{lf} \cos(\beta - \delta) + F_{cf} \sin(\beta - \delta)}{m} \quad (2.17)$$

Equations (2.15) to (2.17) represent the vehicle motion. The lateral motion is given by (2.15) and (2.16). The longitudinal motion is given by (2.17).

2.2 Decoupled Vehicle Model

It can be observed from (2.17) that the longitudinal motion is affected by the lateral motion of the vehicle (from β , δ , F_{cr} , F_{cf}). This means that there will be a change in velocity during a lane change or while turning. In order to avoid this effect, the recent work in [49] suggests a method to decouple the longitudinal motion from the lateral motion. This is achieved by applying the traction force in the form

$$F_{lf} = \frac{mu - F_{cf} \sin(\beta - \delta) - F_{cr} \sin(\beta)}{\cos(\beta - \delta)} \quad (2.18)$$

Substituting this force in (2.17), the resulting longitudinal motion is

$$\ddot{q} = u \quad (2.19)$$

This means that the acceleration of the vehicle can be directly controlled by the input signal u and is independent of the lateral vehicle motion. The remaining equations of the decoupled vehicle model follow if we substitute (2.18) also in (2.15) and (2.16).

$$\dot{\beta} = \frac{F_{cf} + F_{cr} \cos(\delta) - m \cdot u \sin(\beta - \delta)}{m \cdot v \cos(\beta - \delta)} - \dot{\psi} \quad (2.20)$$

$$\ddot{\psi} = \dot{r} = \frac{a \cdot F_{cf} \cos(\delta) - F_{cr} \cdot b}{J} - \frac{a \cdot \sin(\delta) \cdot (F_{cr} \sin(\beta) - m \cdot u + F_{cf} \sin(\beta - \delta))}{\cos(\beta - \delta) \cdot J} \quad (2.21)$$

In addition, the velocities in the X-direction and Y-direction be evaluated as

$$\dot{X} = v \cdot \cos(\beta + \psi) \quad (2.22)$$

$$\dot{Y} = v \cdot \sin(\beta + \psi) \quad (2.23)$$

2.3 Linearized Model

In this section, we evaluate the linearized model [34] of the vehicle around the equilibrium point at the origin. This means that $\delta = \dot{\beta} = \dot{\psi} = \ddot{\psi} = \dot{q} = \ddot{q} = 0$ (straight driving at a constant speed). Then, the linearized model is given by

$$\begin{bmatrix} \dot{\beta} \\ \dot{r} \\ \dot{q} \\ \ddot{q} \end{bmatrix} = \begin{bmatrix} a_{11} & a_{12} & 0 & 0 \\ a_{21} & a_{22} & 0 & 0 \\ 0 & 0 & 0 & 1 \\ 0 & 0 & 0 & 0 \end{bmatrix} \begin{bmatrix} \beta \\ r \\ q \\ \dot{q} \end{bmatrix} + \begin{bmatrix} b_{11} & 0 \\ b_{21} & 0 \\ 0 & 1 \\ 0 & 0 \end{bmatrix} \begin{bmatrix} \delta \\ u \end{bmatrix} \quad (2.24)$$

The variable $r = \dot{\psi}$ is used and the parameters are

$$a_{11} = -\frac{(c_r + c_f)}{mv}, \quad a_{12} = -1 + \frac{(c_r l_r - c_f l_f)}{mv^2}, \quad a_{21} = \frac{(c_r l_r - c_f l_f)}{J},$$

$$a_{22} = -\frac{(c_r l_r^2 + c_f l_f^2)}{Jv}, \quad b_{11} = \frac{c_f}{mv}, \quad b_{21} = \frac{c_f l_f}{J}$$

2.4 Distance from Road and Heading Error Measurement

The models in Section 2.2 and 2.3 only describe the vehicle dynamics. For a lane keeping application, it is also necessary to model the road geometry. Fig. 2 shows a vehicle that has to follow a guideline (road).

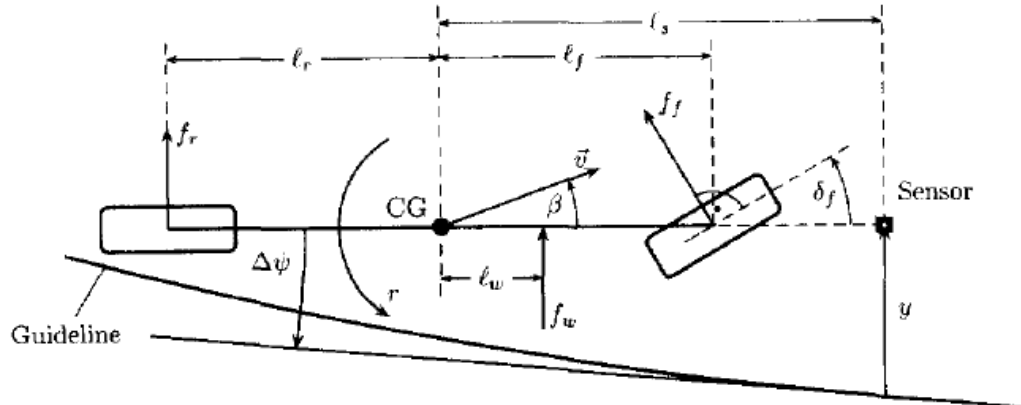


Figure 2.2: Vehicle on a road

The figure assumes that the vehicle has a sensor to measure the distance from the guideline. This sensor is at a distance l_S from the COG. The important variables in this figure are the distance y_S of the sensor from the guideline, the distance y_R of the COG from the centerline and the heading error $\Delta\psi$ (difference between road heading angle and vehicle heading angle). In addition, the road curvature (change of road angle per traveled arc length) is called ρ .

In a linear model, the road geometry is modeled by the following equations:

$$\Delta\dot{\psi} = r - v \rho \quad (2.25)$$

$$\dot{y}_S = v \cdot (\beta + \Delta\psi) + l_S \cdot r \quad (2.26)$$

(2.25) shows that the heading error changes with the difference between the rotational velocity of the vehicle r and the rotational velocity of the road traveled with velocity v . (2.26) shows that the distance of the sensor from the guideline changes with the motion of the COG in direction $(\beta + \Delta\psi)$ (away from the road) and the rotation around the COG with $l_S \cdot r$. The overall linear model consists of (2.24), (2.25) and (2.26). It is sometimes assumed that not the steering angle δ but the steering angle rate $\dot{\delta}$ can be changed as an input signal. In this case, also (2.27) is added to the linear model.

$$\dot{\delta} = u_r \quad (2.27)$$

For the nonlinear model, it is more difficult to include the road geometry in the model. Most of the work in the literature uses the linear model for the road geometry in (2.25) and (2.26). However, we will show in the simulation study in Section 2.5 that this model is not realistic. This means that results obtained with the linear model of the road geometry might not correct.

We compute the distance from the road using a straight-line approximation of the road trajectory in the X-Y coordinates. That is, the road is represented by a sequence of short straight-line segments. Figure 2.3 illustrates how to compute the distance from one such segment.

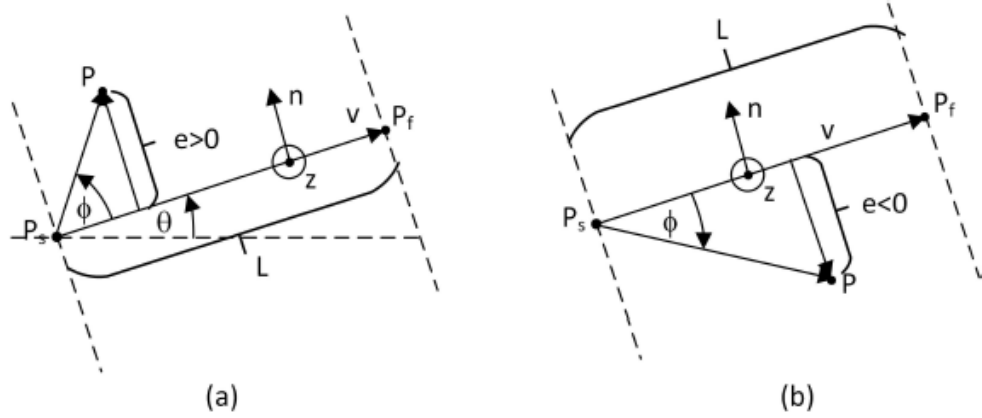


Figure 2.3: Distance computation

We assume that the segment starts at point P_s and ends at point P_f . The vehicle COG or vehicle sensor are located at point P . The length of the line segment is L . Then, the vectors seen in the figure follow:

$$v = L \cdot \begin{bmatrix} \cos(\theta) \\ \sin(\theta) \end{bmatrix} \quad (2.28)$$

$$n = \frac{1}{L} \cdot \begin{bmatrix} 0 \\ 0 \\ 1 \end{bmatrix} \otimes v = \frac{1}{L} \cdot \begin{bmatrix} 0 \\ 0 \\ 1 \end{bmatrix} \otimes \begin{bmatrix} v \\ 0 \end{bmatrix} = \frac{1}{L} \cdot \begin{bmatrix} -\sin(\theta) \\ \cos(\theta) \\ 1 \end{bmatrix} \quad (2.29)$$

$$w = P - P_s \quad (2.30)$$

The distance of point P from the road can now be computed as

$$e = \frac{\langle w, n \rangle}{|n|}. \quad (2.31)$$

This distance (error) can be positive or negative. It is positive in the case of Fig. 2.3 (a) and negative in the case of Fig. 2.3 (b). We can also find the heading error $\Delta\Psi = \phi$ in Fig. 2.3. It holds that

$$\sin(\phi) = \frac{e}{|P - P_s|} \quad (2.32)$$

Together, we use the nonlinear model with the equations in (2.15) to (2.17), the distance error computation in (2.31) and the heading error computation in (2.32).

2.5 Simulations, comparison of decoupled vehicle model and linearized vehicle model

2.5.1 Vehicle Parameters

The study in this thesis uses two different sets of vehicle parameters. The first set of parameters belongs to a city bus [54] and the second set of parameters belongs to a passenger car [51]. The relevant parameters are listed in Table 2.1.

Table 2.1: Vehicle Parameters

Parameters	Bus	Passenger Car
c_f [N/rad]	198000	286400
c_r [N/rad]	470000	194800
m [kg]	16000	2023
J [kg m ²]	173600	6286
l_f [m]	3.67	1.26
l_r [m]	1.93	1.9

2.5.2 Motion on Straight Road

We perform a simulation experiment on a straight road. The vehicle travels at a constant speed of $v = 20$ m/s and the steering angle is adjusted such that the vehicle moves to the left and right on the road. Experiments for different steering angle profiles and different steering angle magnitudes are conducted.

The first experiment periodically changes the steering angle up to a magnitude of 5° . The simulation results with the signals β (side-slip angle), $r = \dot{\psi}$ (yaw rate), $\Delta\psi$ (heading angle error), y_S (distance error at preview distance), y_R (distance at COG) and δ (steering angle) are shown for the bus and the passenger vehicle in Fig. 2.4 and 2.5, respectively.

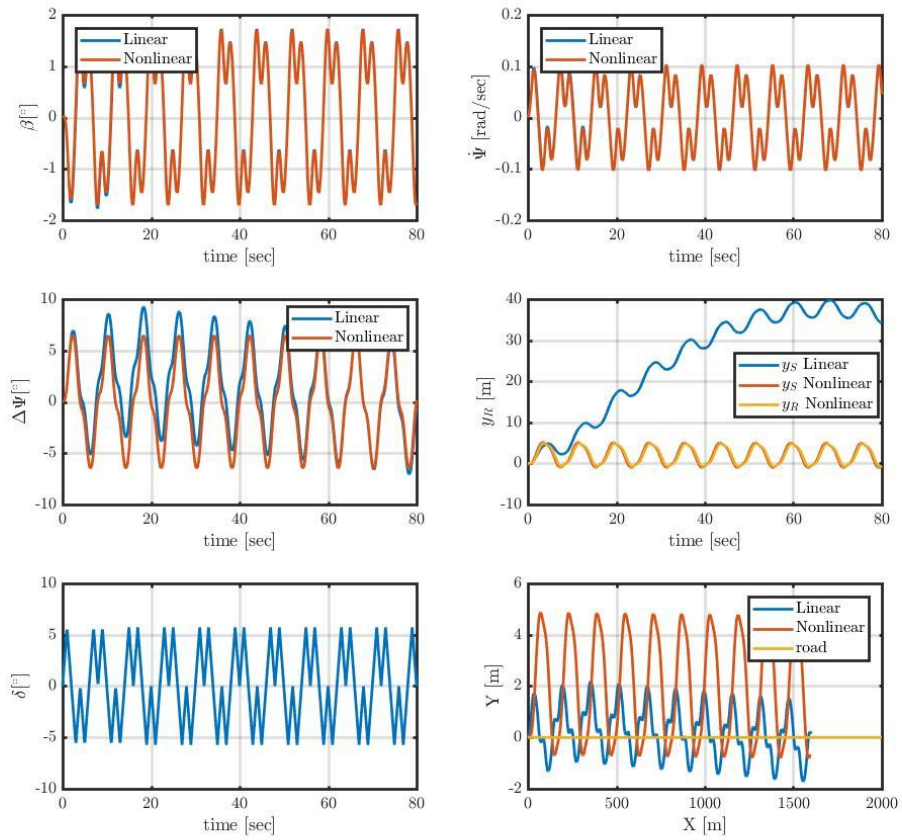


Figure 2.4: Periodic change of the steering angle for the bus up to 5°

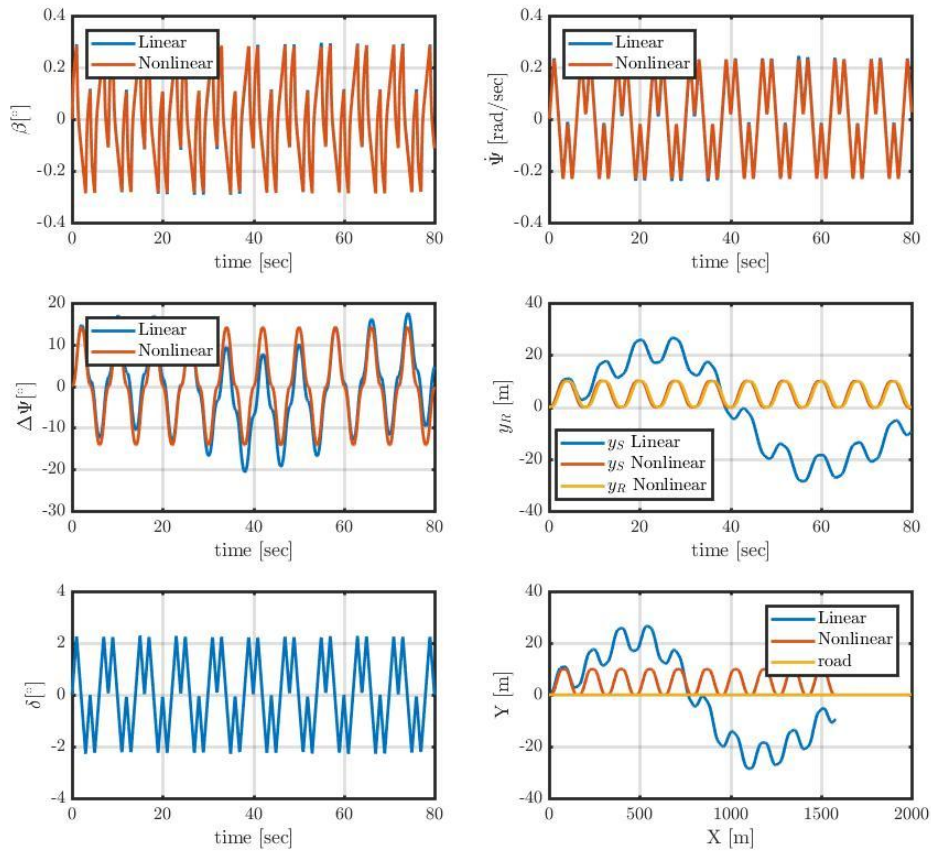


Figure 2.5 : Periodic change of the steering angle for the bus up to 2°

The simulations in Fig. 2.4 and 2.5 show that the linear model and the nonlinear model have a very similar behavior. This can be seen when observing the signals β and $\dot{\psi}$ which are directly related to the vehicle dynamics. These signals are almost identical for the linear and nonlinear case. Differences can be observed for the signals $\Delta\psi$, y_S , y_R . These signals are related to the road geometry. It can be seen that deviations are observed between the linear and nonlinear model as time passes. The main reason is that the linear model only evaluates y_S locally based on the integration of (2.26). Differently, the exact position of the vehicle and the road are used when computing y_S for the nonlinear model.

The next simulation experiment uses the same input signal δ with a larger magnitude up to 20° in Fig. 2.6 for the bus.

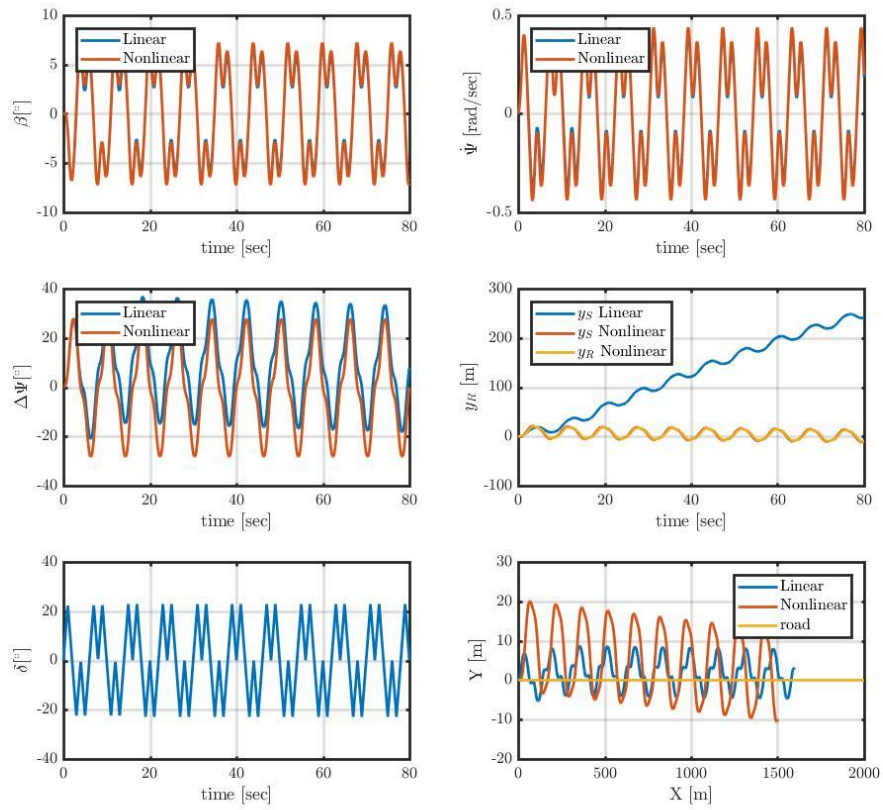


Figure 2.6 : Periodic change of the steering angle for the bus up to 20°

The result is very similar to Fig. 2.4 and 2.5. Only the observed signal magnitudes are larger due to the larger input signal magnitude. It is interesting to note that the signal $\Delta\psi$ shows a better agreement between linear and nonlinear model than the signal y_s .

The next simulation experiment provides a steering maneuver with left and right turns at a lower frequency compared to the previous experiment. Two different simulations for the bus with different steering angle magnitudes are shown in Fig. 2.7 and 2.8

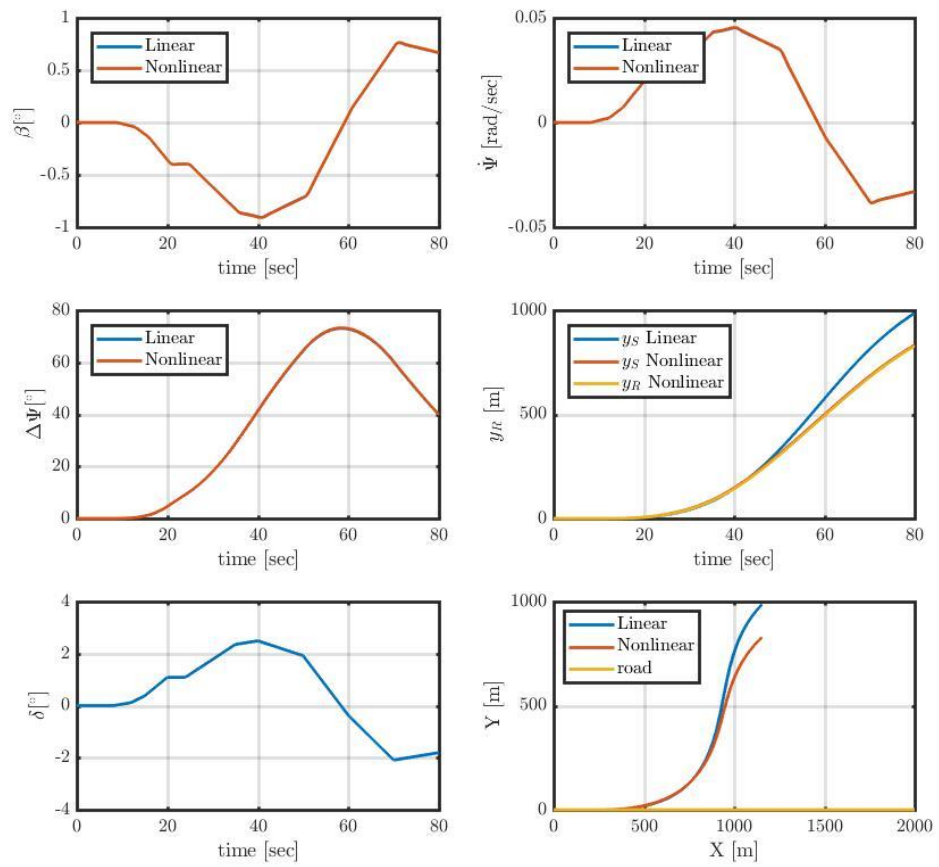


Figure 2.7: Left and right turns of the bus with a steering angle up to 2.5°

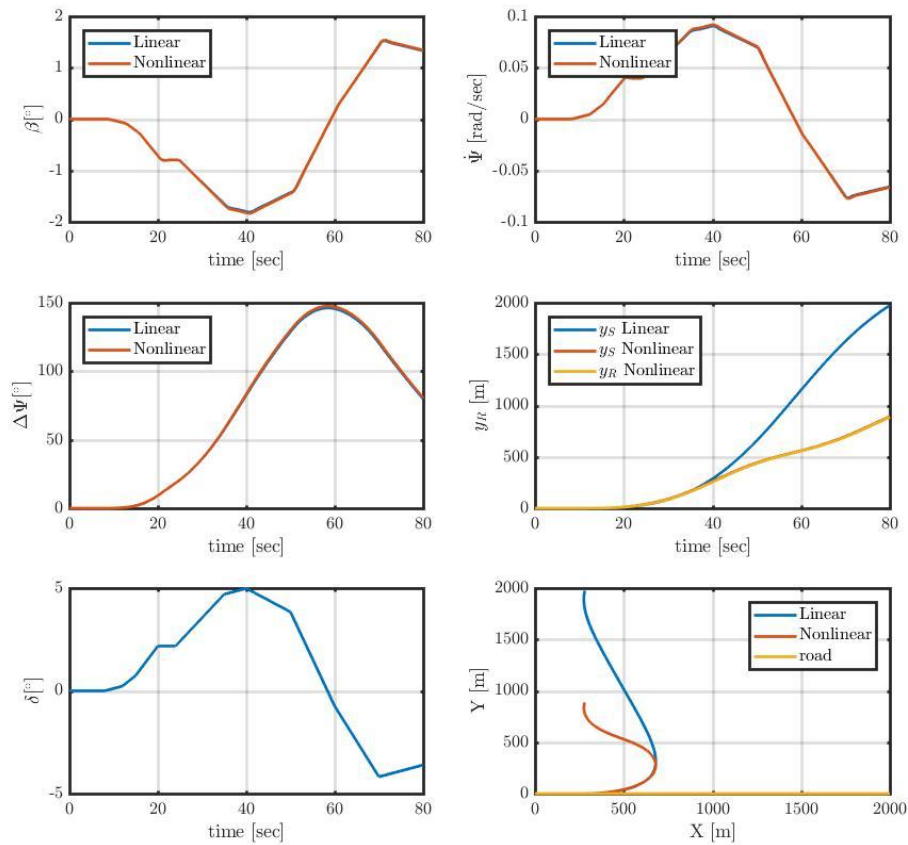


Figure 2.8 : Left and right turns of the bus with a steering angle up to 5°

Again, the signals β , $\dot{\psi}$, $\Delta\psi$ are in very good agreement. An increasing deviation of y_S is observed over time and for larger values of the steering angle.

In summary, we conclude that the linear and nonlinear model are in good agreement. Especially the signals related to the vehicle dynamics (β , $\dot{\psi}$) show almost no deviation. Larger deviations are observed for the variables related to the road geometry if large steering angles are applied and time passes. This is expected due to the local nature of the linear approximation.

2.5.3 Straight Motion and Curved Road

The previous simulation experiments were focused on the change of the vehicle signals during turning maneuvers. This section evaluates the effect of the road geometry by keeping a straight vehicle motion ($\delta = \mathbf{0}$).

First, we look at a road curvature that changes with a frequency of 0.5 rad/sec (Fig. 2.9) and 2 rad/sec (Fig. 2.10) at a speed of $v = 20$ m/s. In this experiment, the road moves to the left/right about 0.5-0.8 m.

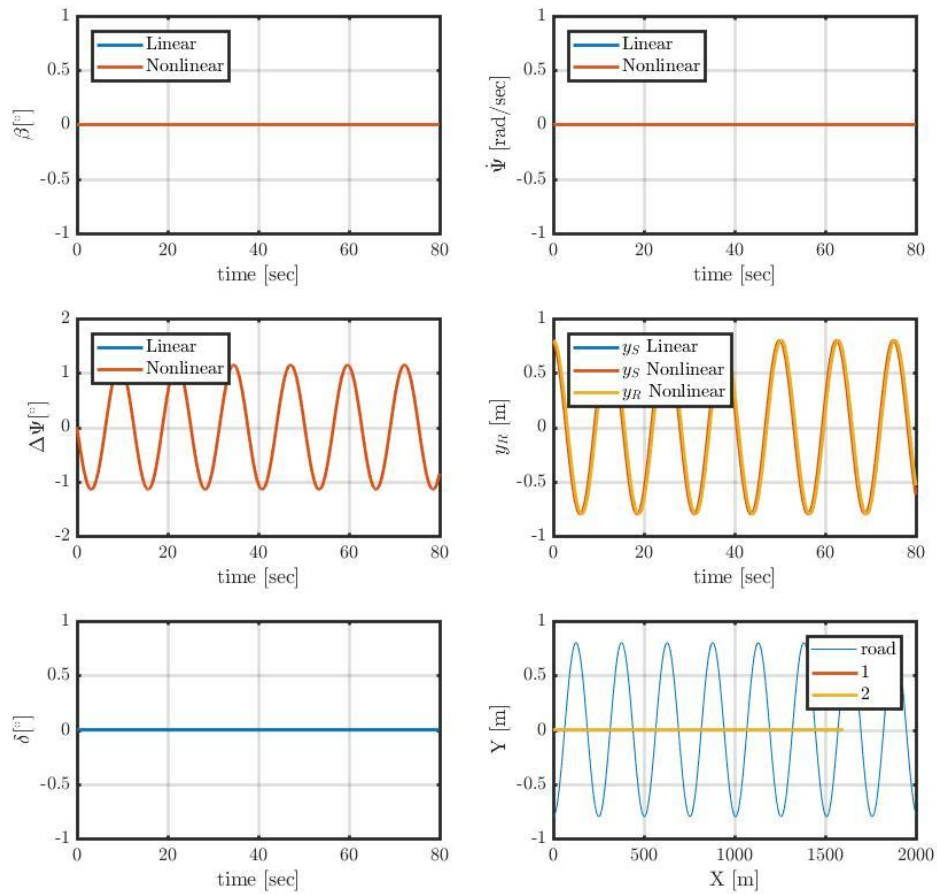


Figure 2.9 : Left and right turns of the road with a frequency of 0.5 rad/sec

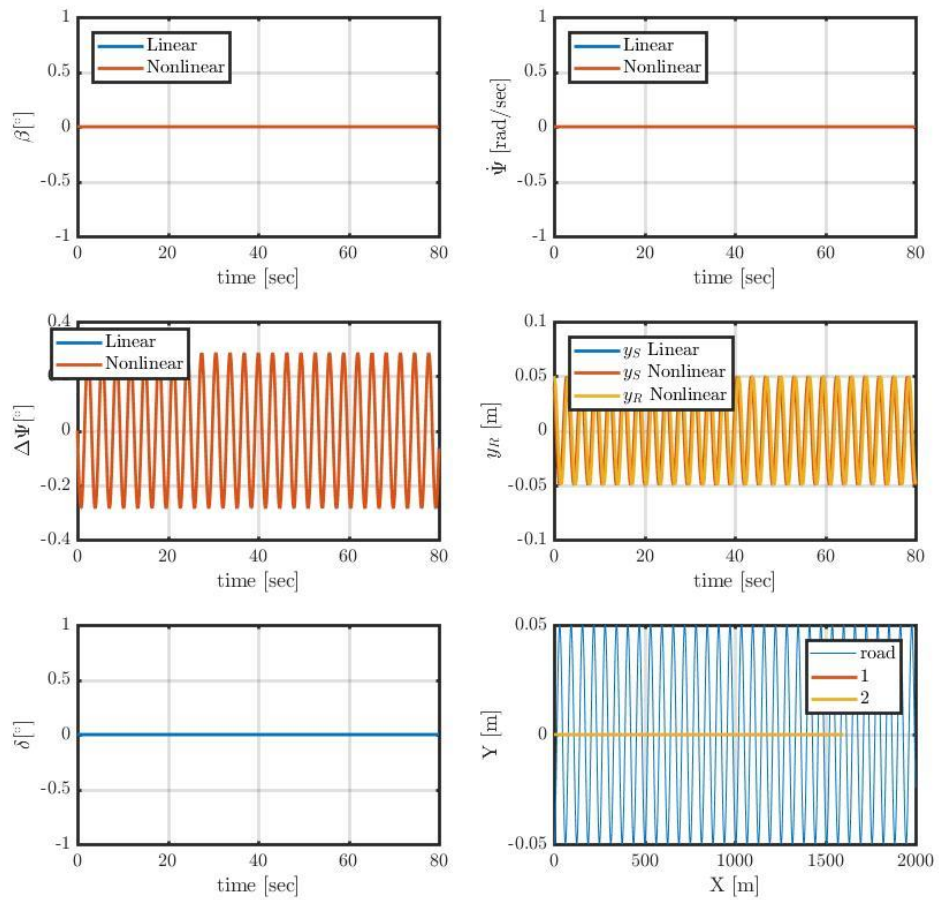


Figure 2.10 : Left and right turns of the road with a frequency of 2 rad/sec

In this experiment, it is clear that the signals β and $\dot{\psi}$ related to the vehicle dynamics are both zero since no turning is performed. The signals related to the road geometry are in good agreement between the linear and nonlinear model.

As the final experiment, we provide a slow change of the road curvature with a left and right turn. The simulation result is shown in Fig. 2.11.

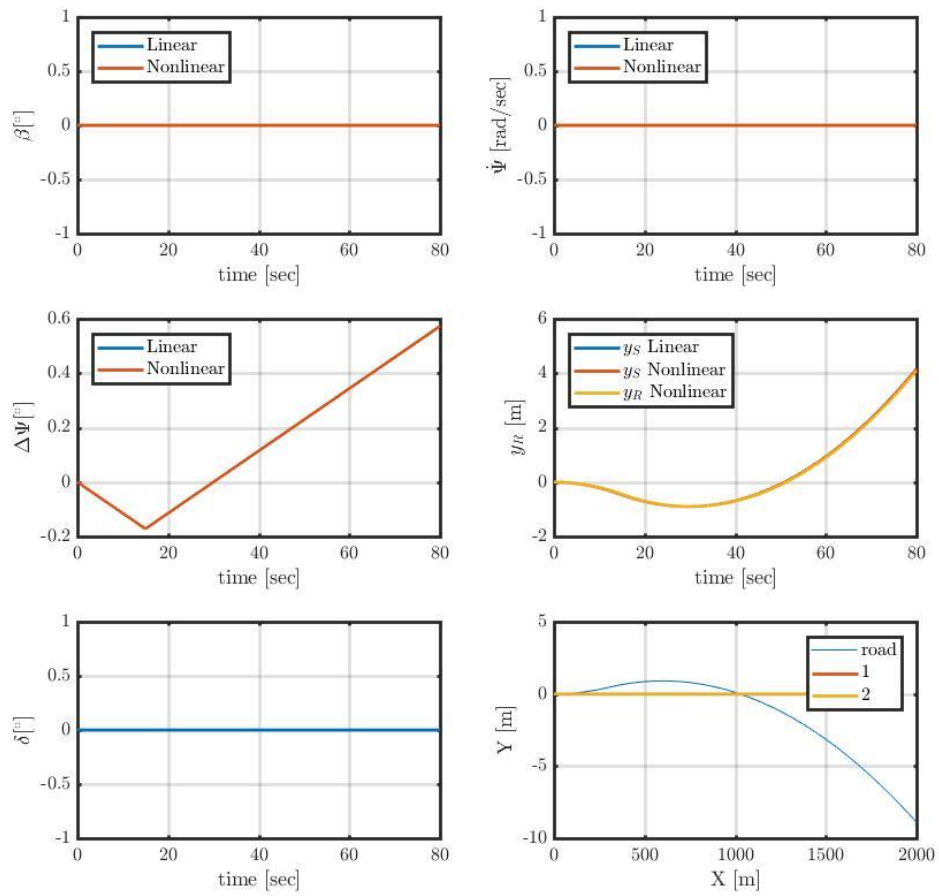


Figure 2.11 : Right and left turn of the road.

The observation is again that the linear and nonlinear model are in good agreement. Together, we conclude that the linear model seems suitable for performing a controller design, whereby deviations in the signals of the road geometry are expected. Furthermore, it must be noted that all comparisons are performed for a constant velocity. The linear model does not capture changes of velocity.

CHAPTER 3

LANE KEEPING ANALYSIS

The previous chapter is about that lane keeping parameters can be specified [50] [34] [52] [53] [54] [55] [56] [57] [58] [59] by using Non-linear Vehicle Model and Linearized Model with Decoupled Vehicle Model. However, it is impossible to determine the optimal control solutions in real-time mode since the parameters that is previously defined as input feedforward and output signals. This chapter involves the description of both of linearized model nonlinear vehicle model to measure distance to road center y , relative yaw angle $\Delta\psi$ and yaw rate r with some important inputs such as front steering angle δ_f and reference road curvature ρ_{ref} .

The chapter is organized as follows. Section 3.1 presents the linearized control model architecture and its results. The representation and results of nonlinear vehicle control model is demonstrated in Section 3.2. In Section 3.3, we can evaluate nonlinear control structure with driving steering model structure.

3.1 Test Setup and General Remarks

We perform two major tests to evaluate the lane keeping algorithms. First, we consider the case of a straight road. The vehicle starts at a distance of 1 m from the centerline of the road and has to approach the road. The performance of this maneuver is evaluated based on oscillations that occur during the approach and the speed of the approach. The basic idea is shown in Fig. 3.1.

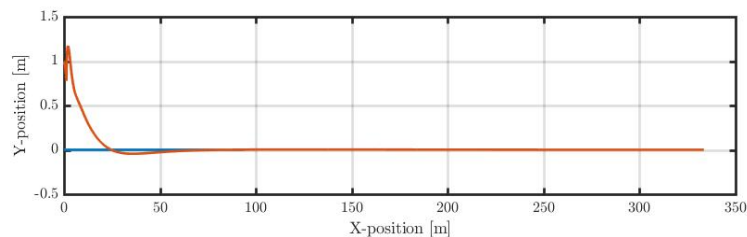


Figure 3.1: Road approach from initial error

In Figure 3.1, the vehicle starts with an error of 1 m and approaches the road center within less than 100 m of driving.

Second, we consider a curved test road with different turns. The road curvature is adjusted to obtain different road radii with a minimum of 80 m. Note that the road radius is the inverse of the road curvature $R = 1/\rho$. The test road is shown in Fig. 3.2.

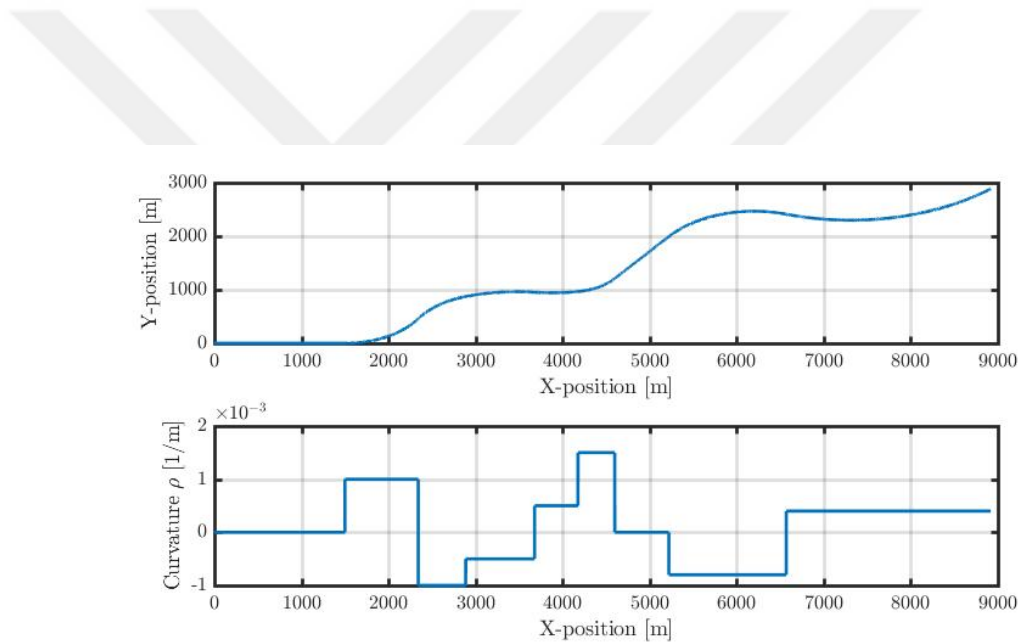


Figure 3.2: Test road with different curvatures.

We note that the test road is generated with step changes of the road curvature in order to give a difficult road profile for the evaluation of the lane keeping algorithms. If the studied lane keeping algorithms show a good performance for this road profile, they will as well show a good performance for smoother road profiles based on clothoid arcs that are used according to some important road standards [51], [58] and [59].

We further provide basic information about the lane keeping control algorithms to be evaluated in the thesis. Lane keeping algorithms are generally based on different measurements of vehicle signals and information about the road geometry. The algorithms studied in this thesis suggest measurements of the yaw rate $\dot{\psi}$, the vehicle velocity v , the heading error $\Delta\psi$, the distance from the road center y_S at the preview distance and the distance from the road center y_R at the COG. Moreover, some of the algorithms directly compute the steering angle δ , whereas some of the algorithms compute the rate of change of the steering angle $\dot{\delta}$. The following evaluation will show which measurements are used for the different control algorithms.

3.2 Linear Controller According to [52]

This control algorithm is taken from [52]. It is based on a linear vehicle model as described in Section 2.3 and 2.4. Details about the controller and the simulation study are given in the following subsections.

3.2.1 Controller Structure

The controller is based on a feedback of the vehicle yaw rate and the distance error y_S at the preview distance. The controller computes the rate of change of the steering angle $\dot{\delta}$. The overall control law in the Laplace domain is as follows.

$$s \delta(s) = -k_r r(s) - C_y(s) y_s(s) \quad (3.1)$$

$C_y(s)$ is a transfer function that has to be designed according to the vehicle parameters. In this thesis,

$$C_y(s) = \frac{0.5 \cdot s + 1}{0.1 \cdot s + 1} \cdot \left(0.5 + \frac{0.3}{s} + \frac{0.03}{s^2} \right) \quad (3.2)$$

has been found suitable for both the bus parameters and the passenger vehicle parameters. In addition, $k_r = 0.89$ is used as in [52]. The controller in (3.2) has the advantage of using a double-integrator for controlling the distance error y_s . As a result, a zero steady-state error is expected when following curved roads with a constant and linearly changing curvature [51].

3.2.2 Evaluation for the Bus Parameters

Next, the controller in (3.1) is evaluated using the test setup described in Section 3.1 for the bus parameters. In all simulations, a comparison of the closed loop system with the linear model and the nonlinear model are shown.

The response to an initial displacement error of 1 m at a speed of $v = 20$ m/s is shown in Fig. 3.3. It can be seen that the behavior of the linear model and the nonlinear model are similar. It is further the case that the vehicle approaches the road centerline with some overshoot within about 3 s, which corresponds to a traveled distance of about 60 m. It is interesting in this experiment that the distance error y_R is smaller than the distance error y_S . This is a positive effect of this controller since it is actually desired that the COG moves on the road centerline. y_S is only the error preview that is used for control.

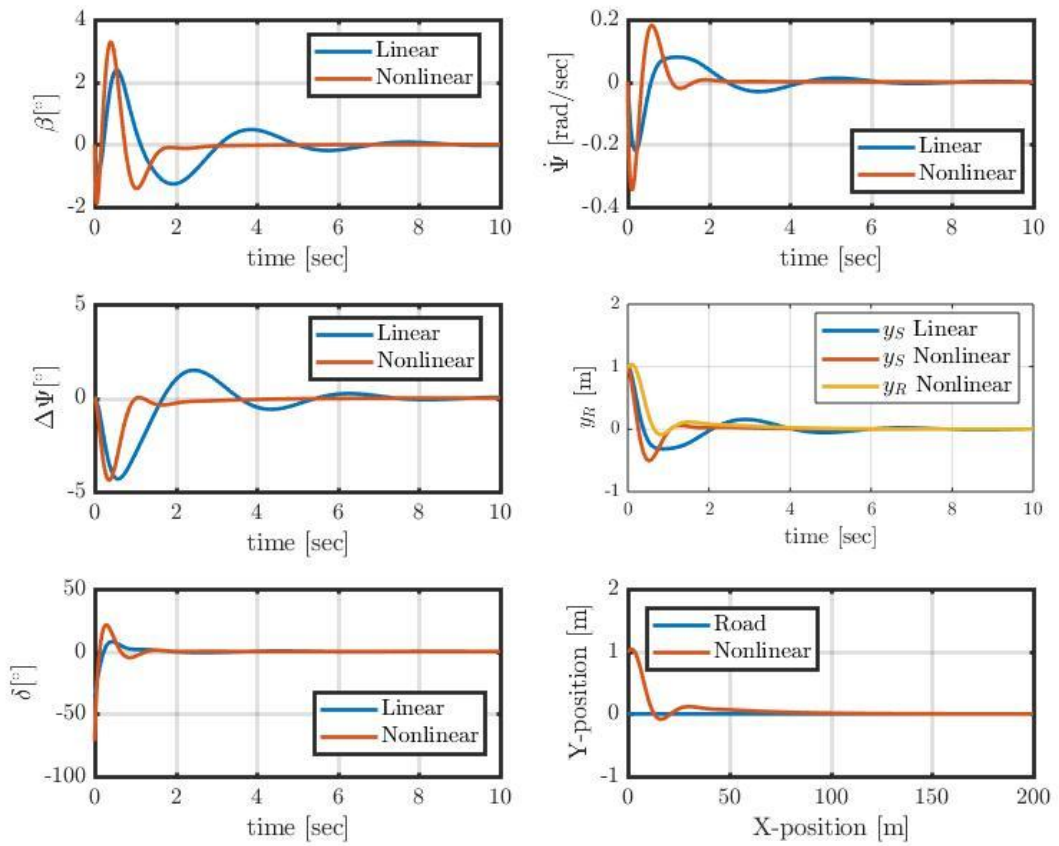


Figure 3.3: Response for an initial displacement error of 1 m (bus parameters)

We next perform simulation experiment for the test road described in Section 3.1 at different speeds of $v = 10, 20, 30$ m/s. In the first set of experiments, the preview distance $l_S = 12$ m is chosen (Figure 3.3 to 3.5). The second set of experiments uses the preview distance $l_S = 6$ m.

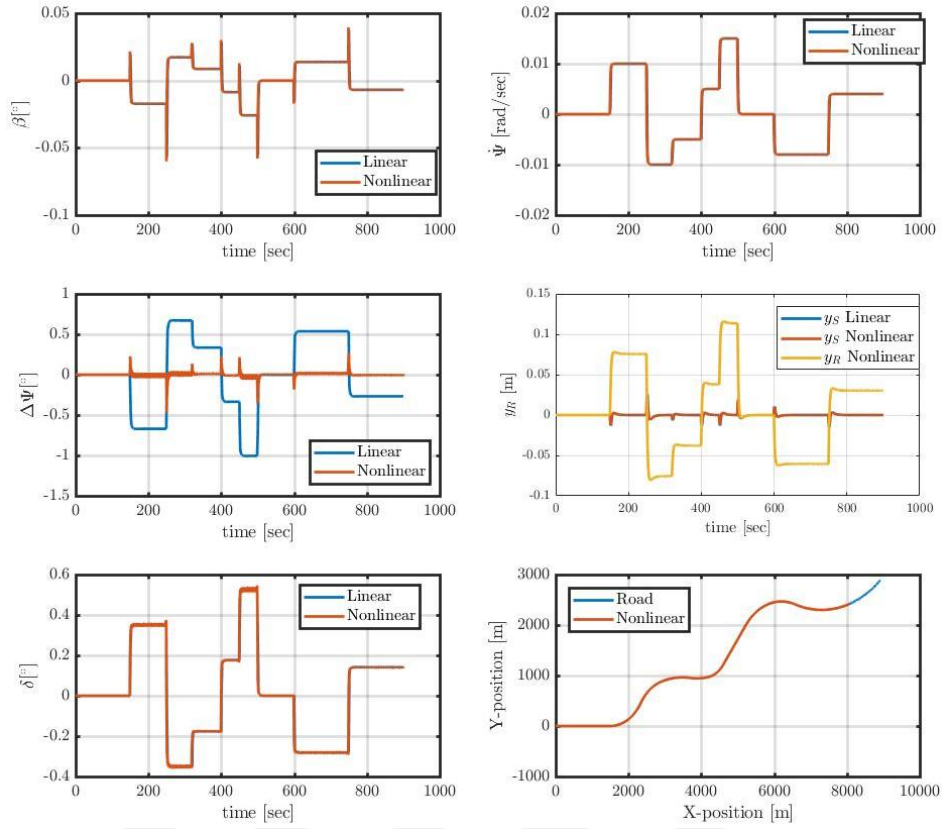


Figure 3.4: Following the test road at $v = 10$ m/s with $l_s = 12$ m (bus parameters)

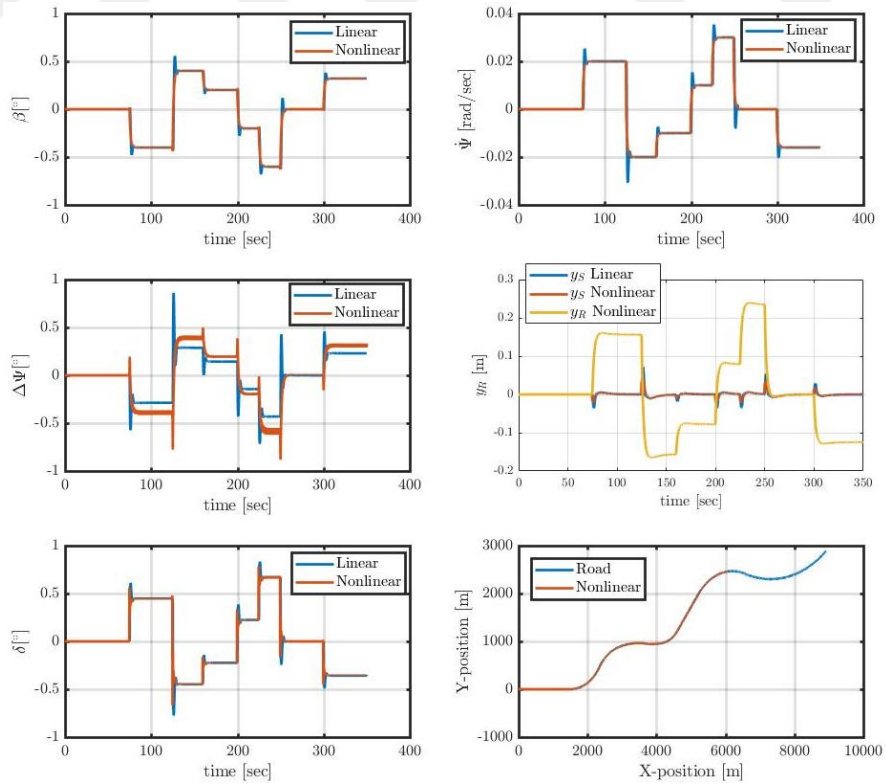


Figure 3.5: Following the test road at $v = 20$ m/s with $l_s = 12$ m (bus parameters)

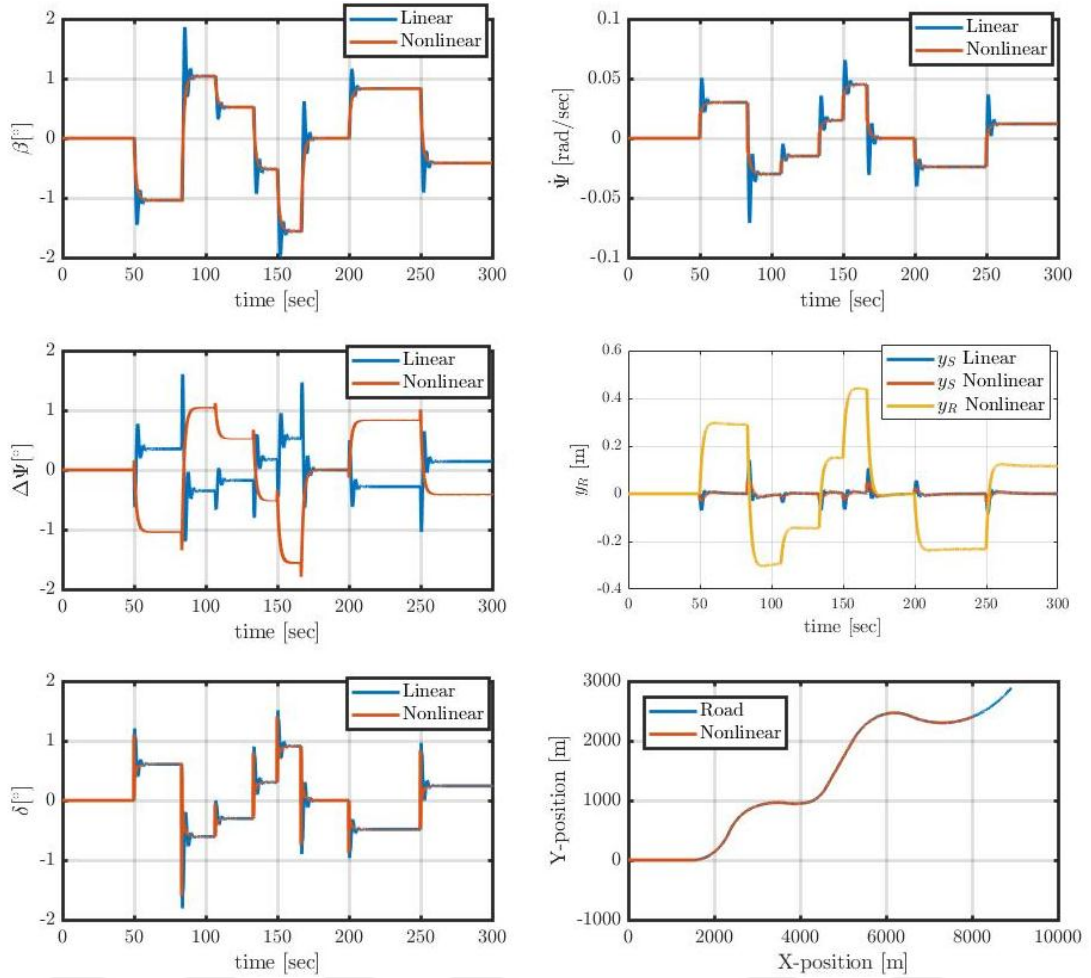


Figure 3.6: Following the test road at $v = 30$ m/s with $l_S = 12$ m (bus parameters)

It can be seen from the simulations in Figure 3.3 to 3.6 that increasing displacement errors y_R of the COG and oscillations in the steering angle signal δ are observed when increasing the vehicle speed. This is an expected result since the same vehicle travels the same road faster, leading to increased lateral forces that impact on the vehicle motion. The most interesting result is that displacement error y_S at the preview distance remains small for all speeds. This is due to the fact that the controller tries to regulate y_S to zero. Nevertheless, this is an undesired result since the actual objective is to make y_R equal to zero. It has to be noted that the entire existing literature neglects this fact and assumes that y_R will be small as long as y_S is small. However, this assumption is invalid as can be seen from the simulation results.

The difference between y_R and y_S depends on the preview distance l_S . Because of this reason, we perform additional simulation experiments with a reduced preview

distance $l_s = 6$ m.

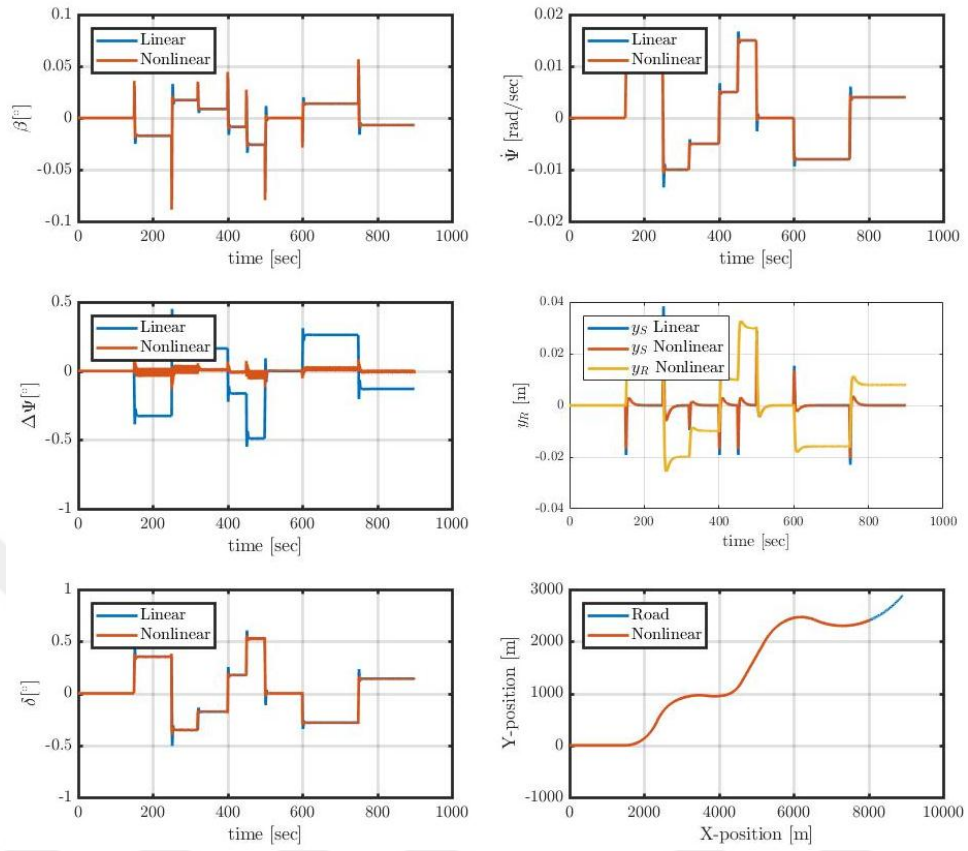


Figure 3.7: Following the test road at $v = 10$ m/s with $l_s = 6$ m (bus parameters)

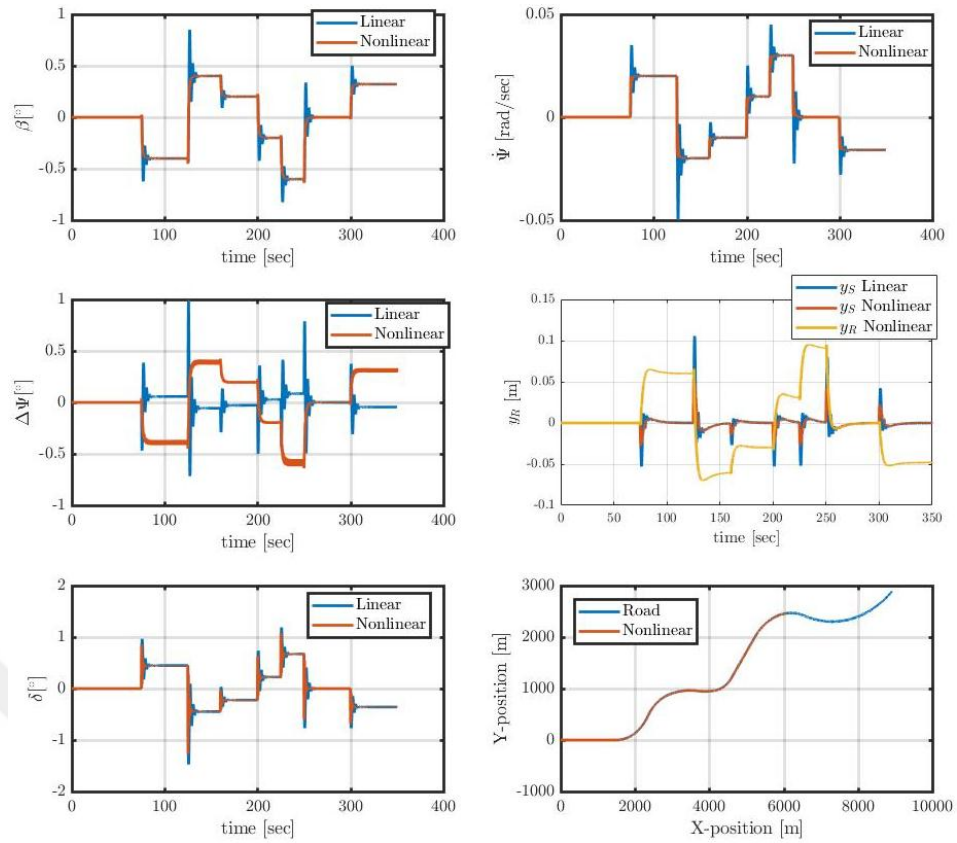


Figure 3.8: Following the test road at $v = 20$ m/s with $l_S = 6$ m (bus parameters)

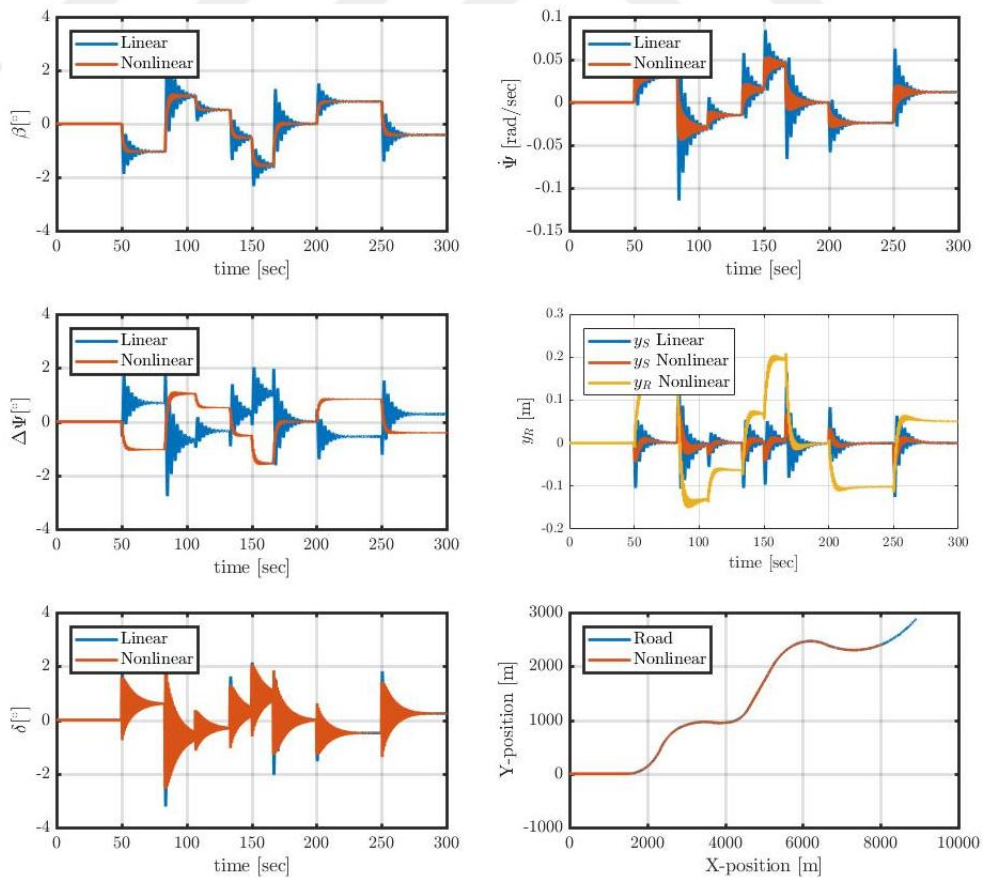


Figure 3.9: Following the test road at $v = 30$ m/s with $l_S = 6$ m (bus parameters)

It can be seen from Fig. 3.6 to 3.9 that the difference between y_R and y_S is indeed reduced for the smaller preview distance l_S . However, using the controller in (3.1) introduces increased oscillations for a decreased preview distance, which is an undesired effect.

In summary, the linear controller in [52] achieves a satisfactory performance for the bus parameters at moderate speeds up to 20 m/s if a large enough preview distance is chosen. A large displacement error and oscillations are observed at high speeds.

3.2.3 Evaluation for the Car Parameters

The previous evaluation was conducted for the bus parameters. Since the same evaluation for the car parameters would be too lengthy, only two representative results are shown. Fig. 3.9 shows that the passenger shows a faster behavior and can approach the centerline in shorter time compared to the bus in Fig. 2. In addition, Fig. 3.11 shows that a shorter preview distance can be used for the passenger car to achieve a smaller displacement error y_R without oscillations compared to the bus in Fig. 3.8.

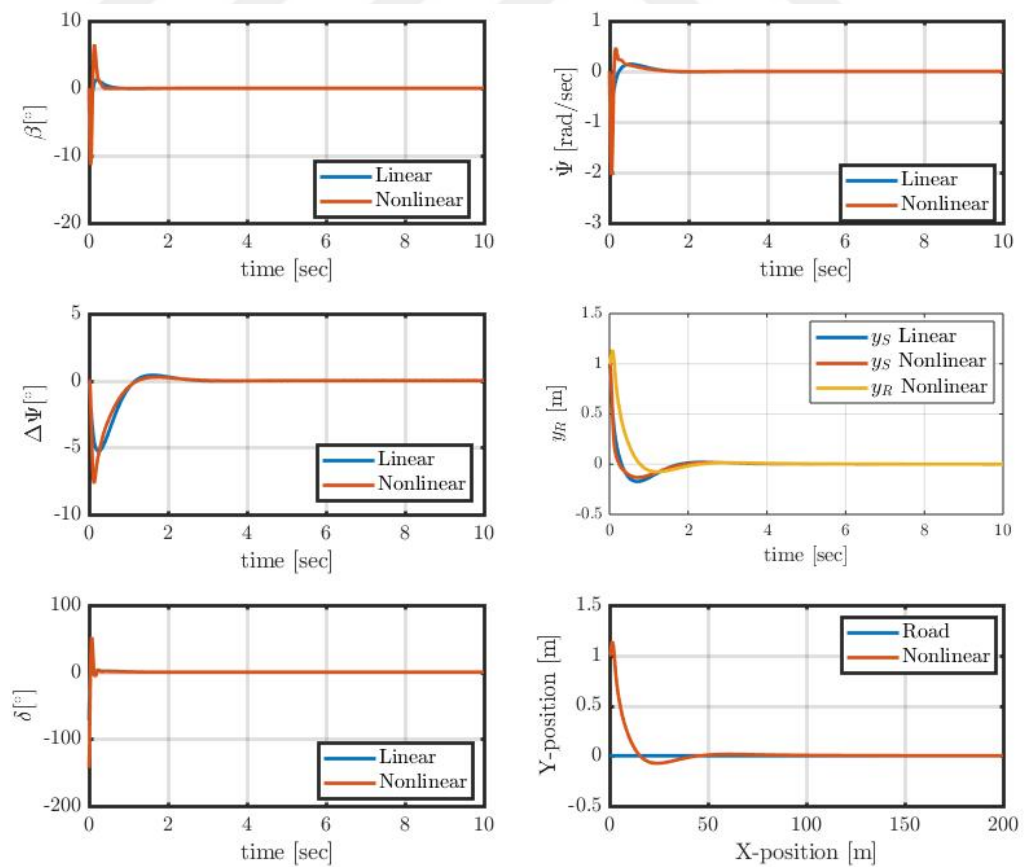


Figure 3.10: Response for an initial displacement error of 1 m (car parameters)

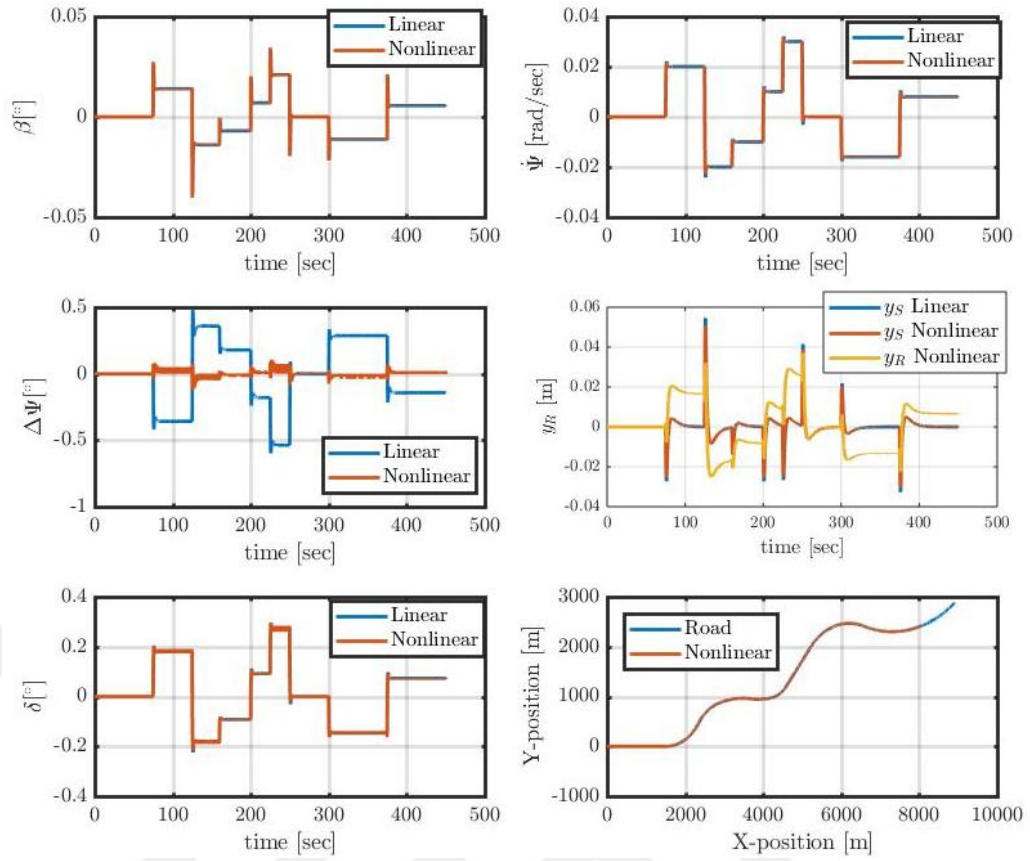


Figure 3.11: Following the test road at $v = 10$ m/s with $l_5 = 6$ m (car parameters)

3.3 Sliding Mode Controller

This control algorithm is taken from [52]. It is based on a linear vehicle model as described in Section 2.3 and 2.4. Details about the controller and the simulation study are given in the following subsections.

3.3.1 Description

The controller in this section uses the idea of sliding mode control. It is based on the measurement of the displacement error y_S and the yaw rate $\dot{\psi}$ and computed the rate of change of the steering angle $\dot{\delta}$. The basic structure of the controller is shown in Fig. 3.12.

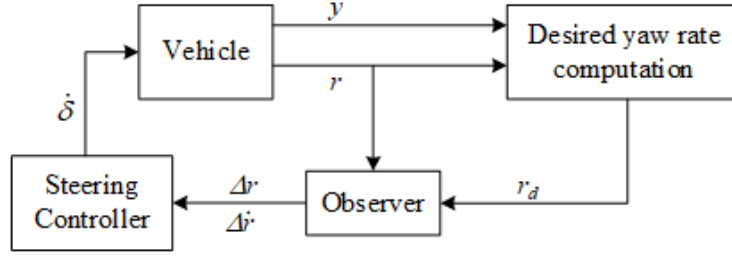


Figure 3.12: Sliding mode control loop

There are two important components of this control loop. First, the desired yaw rate r_d is computed based on (2.26) as

$$r_d = -\frac{1}{l_s} \cdot (v \cdot (\beta + \Delta\psi) + K \cdot y_S) \quad (3.3)$$

Using r_d , it holds that

$$\dot{y}_S = -K \cdot y_S \quad (3.4)$$

if $r = r_d$. K specifies the desired rate of convergence of y_S . Second, the steering controller is realized using sliding mode control such that the condition $r = r_d$ is achieved. [52] defines the yaw rate error $\Delta r = r - r_d$ and applies sliding mode control with the sliding surface

$$S = c \cdot \Delta r + \Delta \dot{r} \quad (3.5)$$

c determines the convergence of Δr on the sliding surface $S = 0$. Using S as defines in (3.5), the control input (rate of change of the steering angle) is defines as

$$\dot{\delta} = -M_u \cdot \text{sign}(S) \quad (3.6)$$

As a result, $\dot{\delta}$ switches between positive and negative values depending on the variable S . In order to avoid chattering (fast switching), (3.6) is further replaced by the more practical realization of the control signal

$$\dot{\delta} = -M_u \cdot \tan^{-1} \left(10 \cdot \frac{2}{\pi} \cdot S \right) \quad (3.7)$$

The remaining problem for the realization of (3.5) is the computation of $\Delta \dot{r}$, which requires the time derivative of the yaw rate r . Since r is a measured signal, obtaining its time derivative in practice is not possible due to noise. Hence, it is suggested in [52] to realize an observer for the signals Δr and $\Delta \dot{r}$. In order to obtain an observer for the nonlinear system, we define Δr to $z_1 = \Delta r$ and $z_2 = \Delta \dot{r}$. From the state equations of the linear system model in (2.24) to (2.26), we can derive the state space model for z_1 and z_2 in the form

$$\begin{aligned}\dot{z}_1 &= z_2 \\ \dot{z}_2 &= f(\beta, r, \delta, \rho, uf)\end{aligned}\quad (3.8)$$

Introducing the estimates \hat{z}_1 and \hat{z}_2 for these states, the observer system is written as

$$\begin{aligned}\dot{\hat{z}}_1 &= z_2 + M_1 \cdot \overline{z_1} \\ \dot{\hat{z}}_2 &= \hat{f} + M_1 \cdot M_2 \cdot \overline{z_1}\end{aligned}\quad (3.9)$$

where $M_1 \gg M_2 > 0$, and \hat{f} is an approximation of f in (3.8). It is shown in [52] that the observer dynamics is stable. The working principle of the real system (3.6) is different from the observer system (3.7)

As a result of the observation, we perform sliding mode control using the observed variables from (3.9) as shown below

$$\hat{S} = c\hat{z}_1 + \hat{z}_2 \quad (3.10)$$

3.3.2 Evaluation for Bus Parameters

We perform the same evaluation as in Section 3.2.2 using the bus parameters. The controller parameters are chosen as $c = 0.6$ and $K = 6.5$ similar to [52]. First, we consider an initial displacement error of 1 m. The resulting simulation is shown in Fig. 3.13.

It can be seen that the vehicle approaches the road center within about 10 s. In addition, there is no overshoot during the approach. The signals of the linear and nonlinear model are very similar. It can further be seen that the distance error y_R of the COG approaches the road center slightly slower than the distance error y_S at the preview distance.

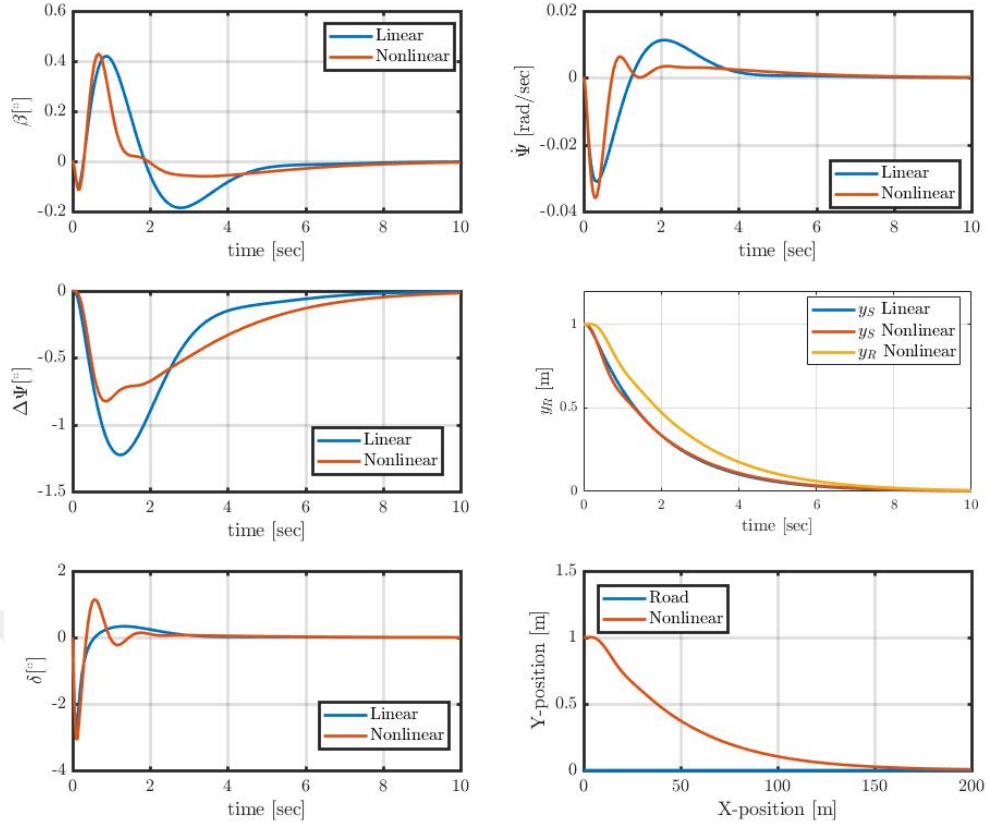


Figure 3.13: Response for an initial displacement error of 1 m (bus parameters)

We next perform simulations for the test road at different speeds $v = 10, 20, 30$ m/s and with different preview distances $l_s = 6$ m, 12 m. The resulting simulation plots are shown in Fig. 3.14 to 3.18.

The general observations are summarized as follows. Similar to Section 3.2, larger displacement errors y_R are observed in the case of a larger pre-view distance and larger velocities. In addition, y_R is generally larger than y_S since y_S is the controlled output signal. It is also the case that larger oscillations of the steering angle δ can be observed for smaller pre-view distances. Furthermore, the linear and nonlinear model again give similar results. Finally, it has to be noted that the feedback loop for the case of $v = 30$ and $l_s = 6$ m is instable such that lane keeping could not be achieved using sliding mode control for large velocities and small pre-view distances.

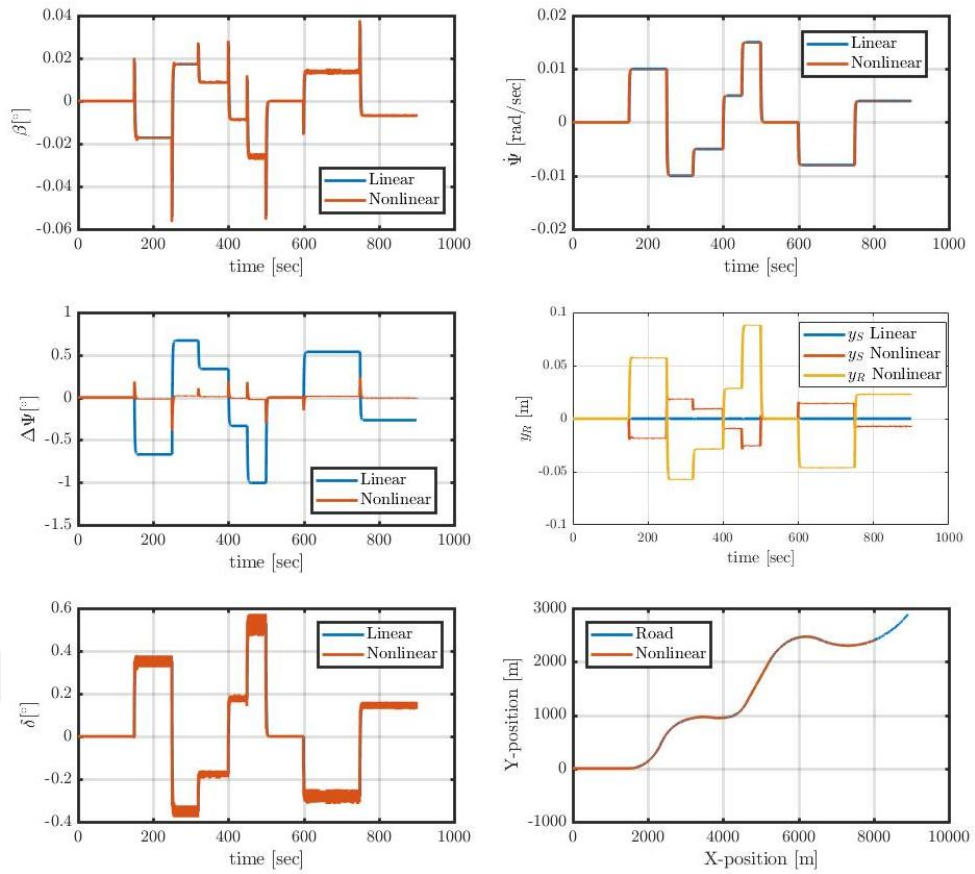


Figure 3.14: Sliding mode control on the test road: $v=10$ m/s; $l_s = 12$ m (bus parameters)

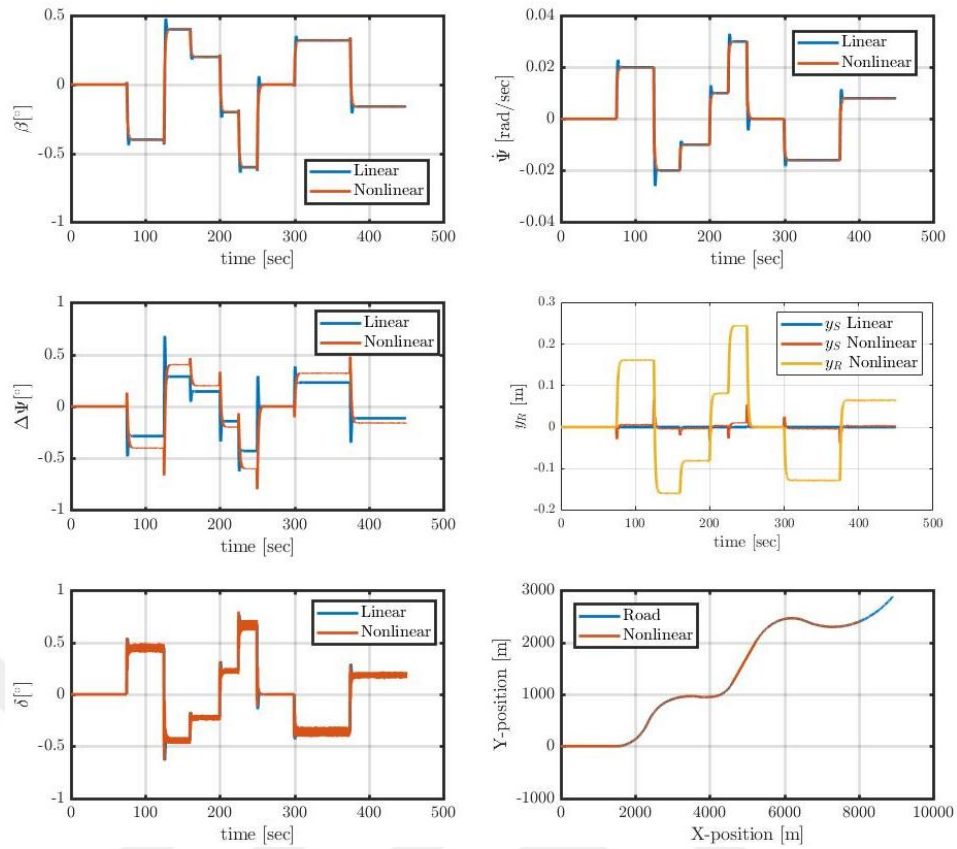


Figure 3.15: Sliding mode control on the test road: $v=20$ m/s; $l_s = 12$ m (bus parameters)

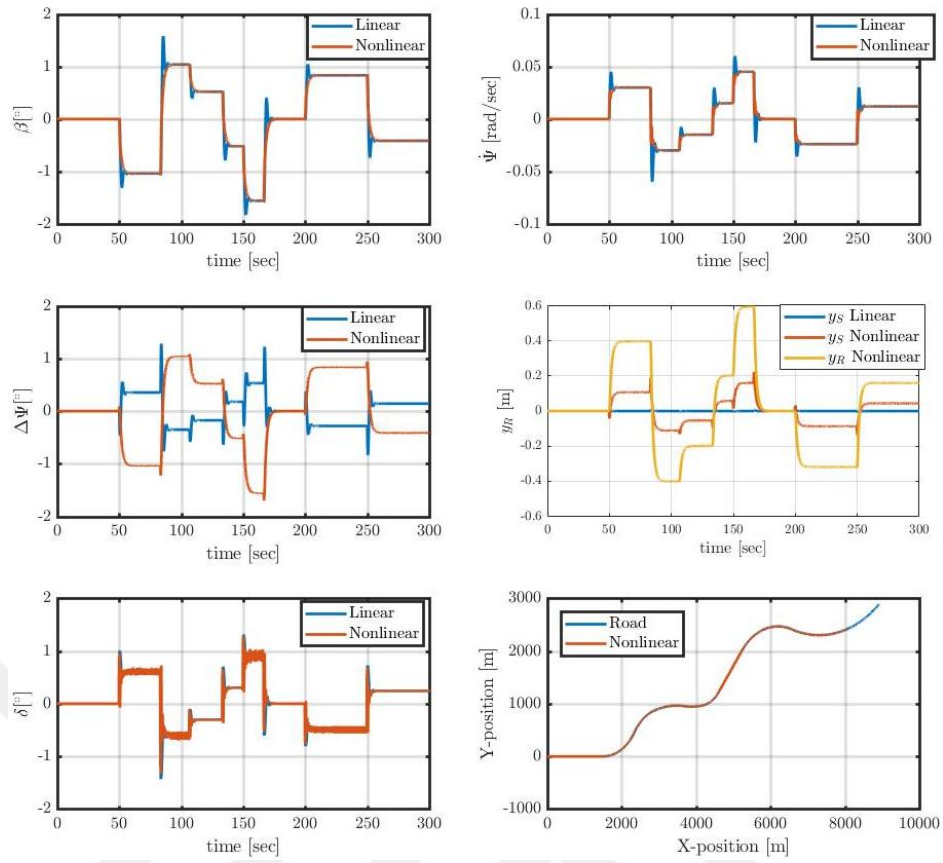


Figure 3.16: Sliding mode control on the test road: $v=30$ m/s; $l_s = 12$ m (bus parameters)

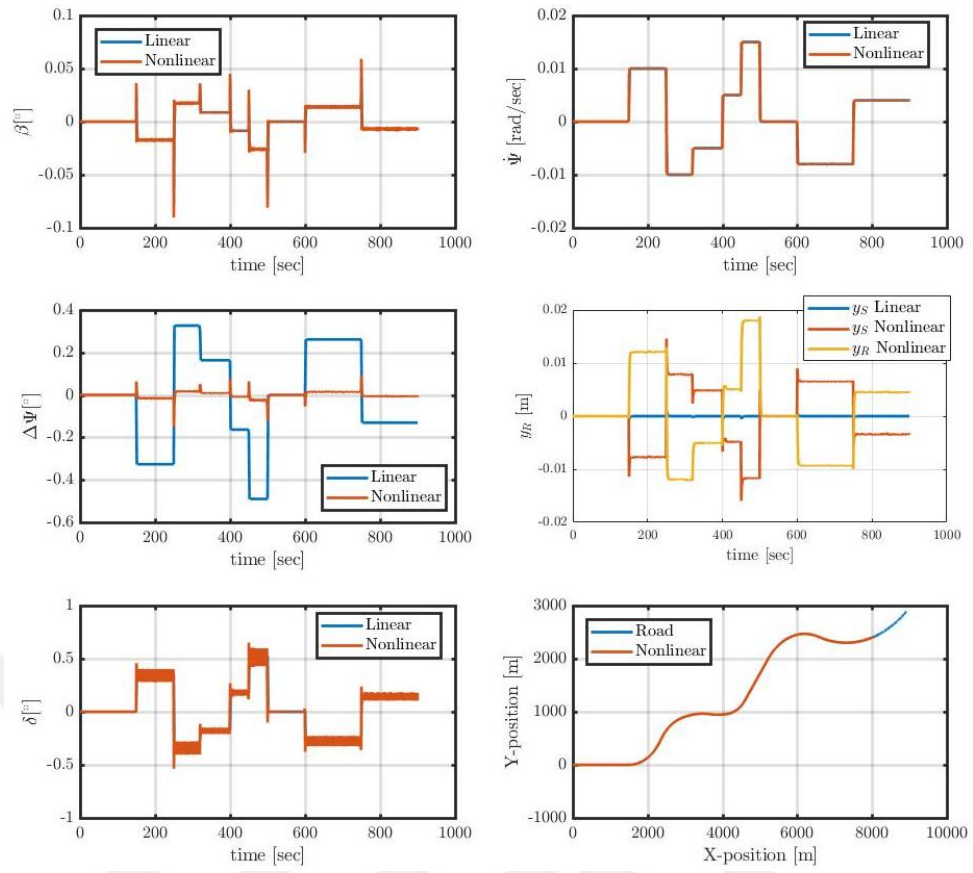


Figure 3.17: Sliding mode control on the test road: $v=10$ m/s; $l_S = 6$ m (bus parameters)

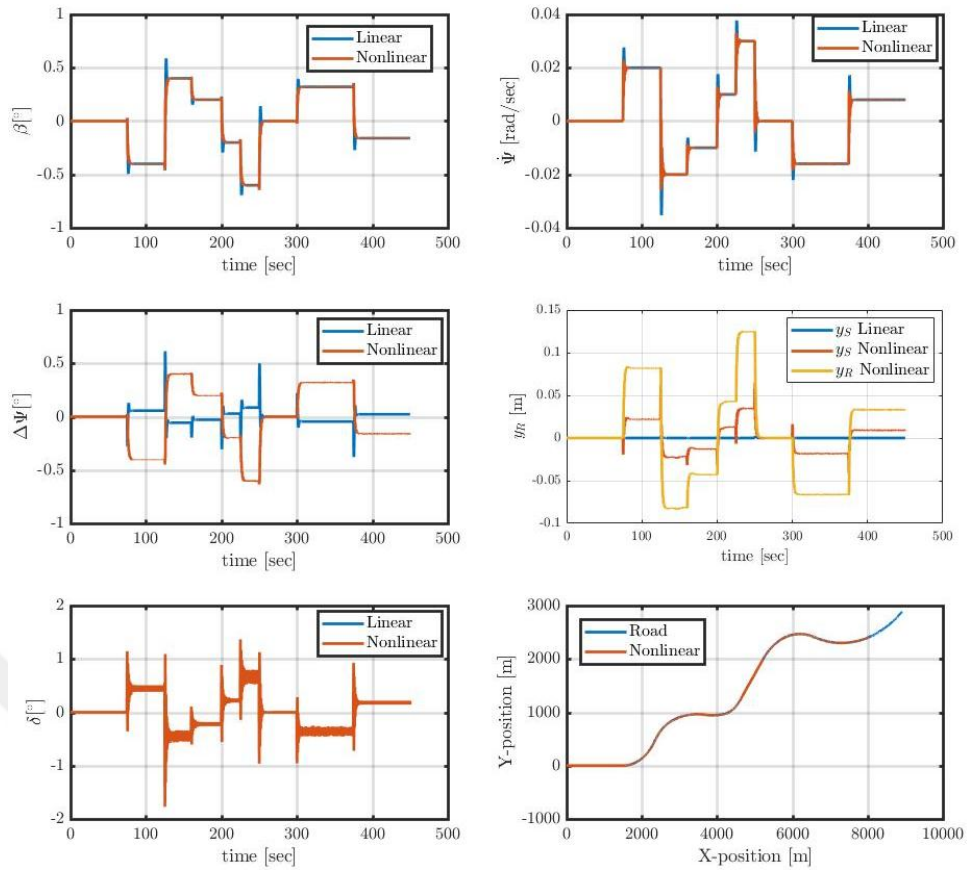


Figure 3.18: Sliding mode control on the test road: $v=20$ m/s; $l_S = 6$ m (bus parameters)

3.3.3 Evaluation for Passenger Car Parameters

We next also show some results for the passenger car parameters. Due to the changed vehicle parameters, also the controller parameters were adjusted to $K = 2$ and $c = 0.3$. Regarding the non-zero initial condition, Fig. 3.19 shows that convergence to the road center is achieved within about 10 s, whereby oscillations in the steering angle are observed.

Regarding road following, Fig. 3.20 shows increased oscillations compared to the case with the bus parameters in Fig. 3.15. Similarly, the displacement error is larger for the case with in Fig. 3.20. That is, sliding mode control as proposed in [52] is more suitable for heavy vehicles such as a bus compared to light vehicles such as passenger cars.

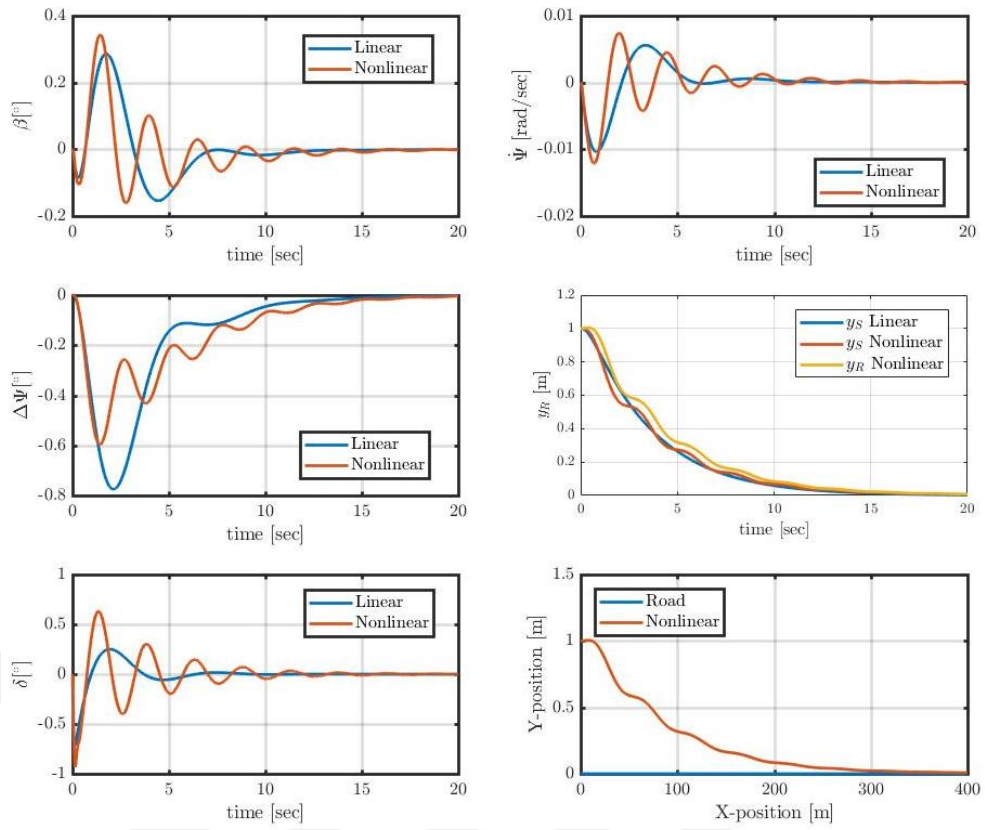


Figure 3.19: Sliding Mode: Response for an initial displacement error of 1 m (car parameters)

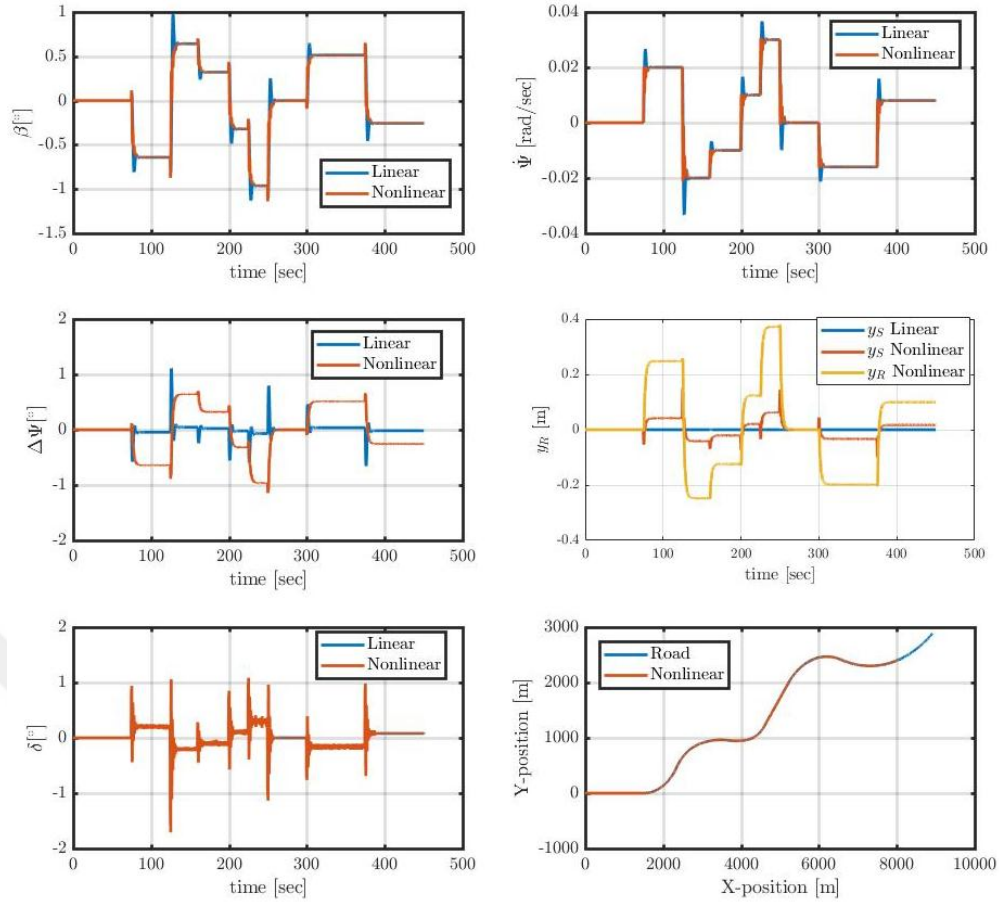


Figure 3.20: Sliding mode control on the test road: $v=20$ m/s; $l_S = 12$ m (car parameters)

3.4 Nested PID Control

This control algorithm is taken from [34]. It is based on a linear vehicle model as described in Section 2.3 and 2.4. Details about the controller and the simulation study are given in the following subsections.

3.4.1 Description

The work in [34] suggests to use a nested feedback control loop with two controllers $C_1(s)$ and $C_2(s)$ as shown in Fig. 3.21. The measured signals are the same as in Section 3.3: displacement error y_S at the pre-view distance l_S and yaw rate $r = \dot{\psi}$. The computed control signal is the steering angle δ .

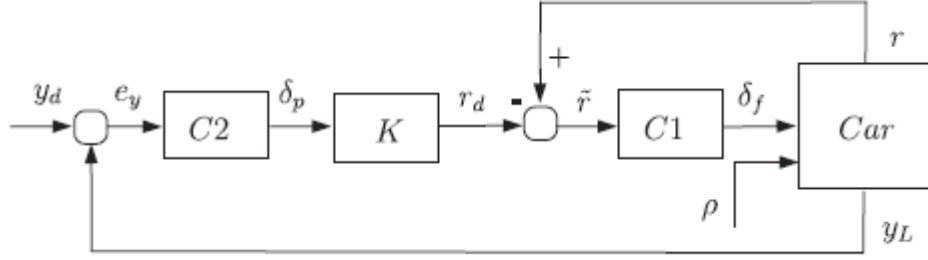


Figure 3.21: Nested feedback loop

The controller $C_2(s)$ measures y_s and determines a predicted steering angle δ_p . This steering angle is converted to a desired yaw rate r_d by multiplication with K . Then, the yaw rate error $\tilde{r} = r_d - r$ is computed and controlled by the controller $C_1(s)$. The road curvature ρ is considered as a disturbance to the control system. The realization of the two controllers is as follows. $C_2(s)$ is realized as a PI controller in the form

$$C_1(s) = K_{P1} + \frac{K_{I1}}{s} \quad (3.11)$$

$C_2(s)$ is realized as a higher-order controller with two integrators. The idea is to realize a zero steady-state error for linear curvature changes which are frequently observed on roads.

$$C_2(s) = K_{P2} + \frac{K_{I2}}{s} + \frac{K_{I3}}{s^2} \quad (3.12)$$

The parameter values used in this thesis are $K_{P1} = 10, K_{I1} = 10, K_{P2} = 10, K_{I2} = 1, K_{I3} = 0.3, K = 0.05$.

3.4.2 Evaluation for the Bus Parameters

We perform an analogous evaluation to the previous sections. That is, we first evaluate the response to an initial displacement error of 1 m. The simulation result is shown in Fig. 3.22. It holds that the vehicle approaches the road center within about 4 s and without overshoot in the relevant displacement error y_R of the COG. The responses with the linear and nonlinear model are similar.

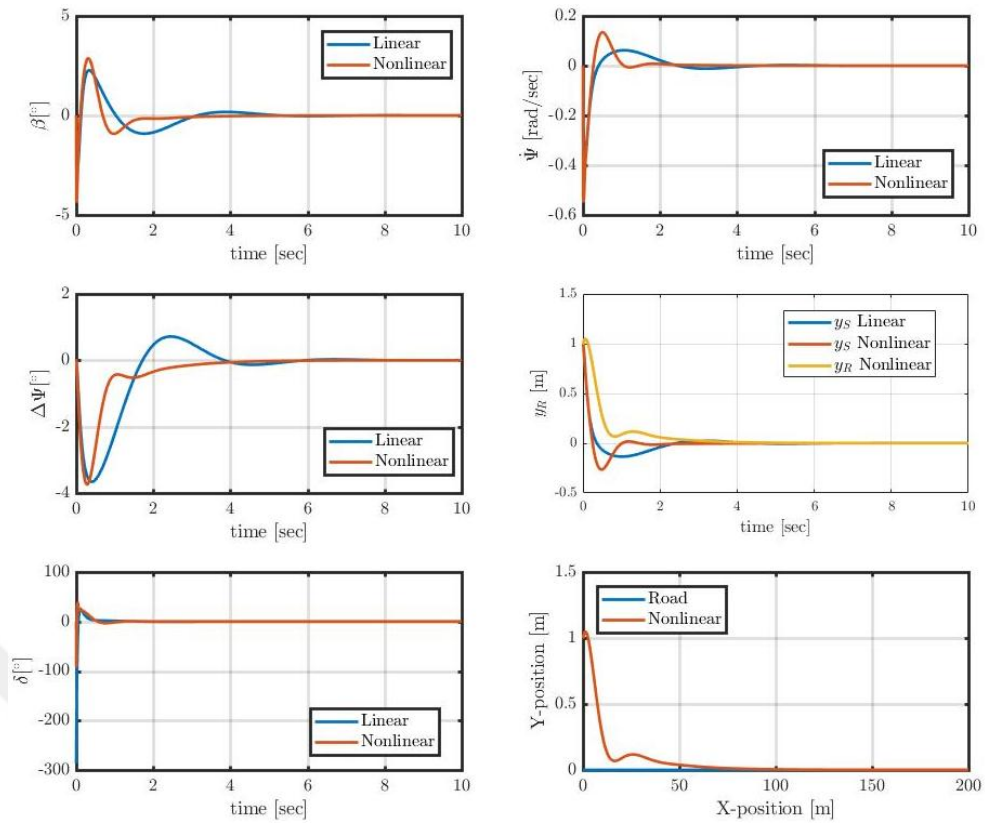


Figure 3.22: Nested PID: Response for an initial displacement error of 1 m (bus parameters)

Next, we consider road tests with different velocities $v = 10, 20, 30$ and pre-view distances $l_s = 6 \text{ m}, 12 \text{ m}$. The resulting simulations are shown in Fig. 3.23 to 3.28. The main observations are as follows. First, it can be seen that larger displacement errors are observed at higher speeds. Second, this controller effectively reduces the displacement error by choosing a smaller pre-view distance up to speeds of 20 m/s. At higher speeds, large oscillations are observed when the pre-view distance is chosen as $l_s = 6 \text{ m}$ (Fig. 3.28).

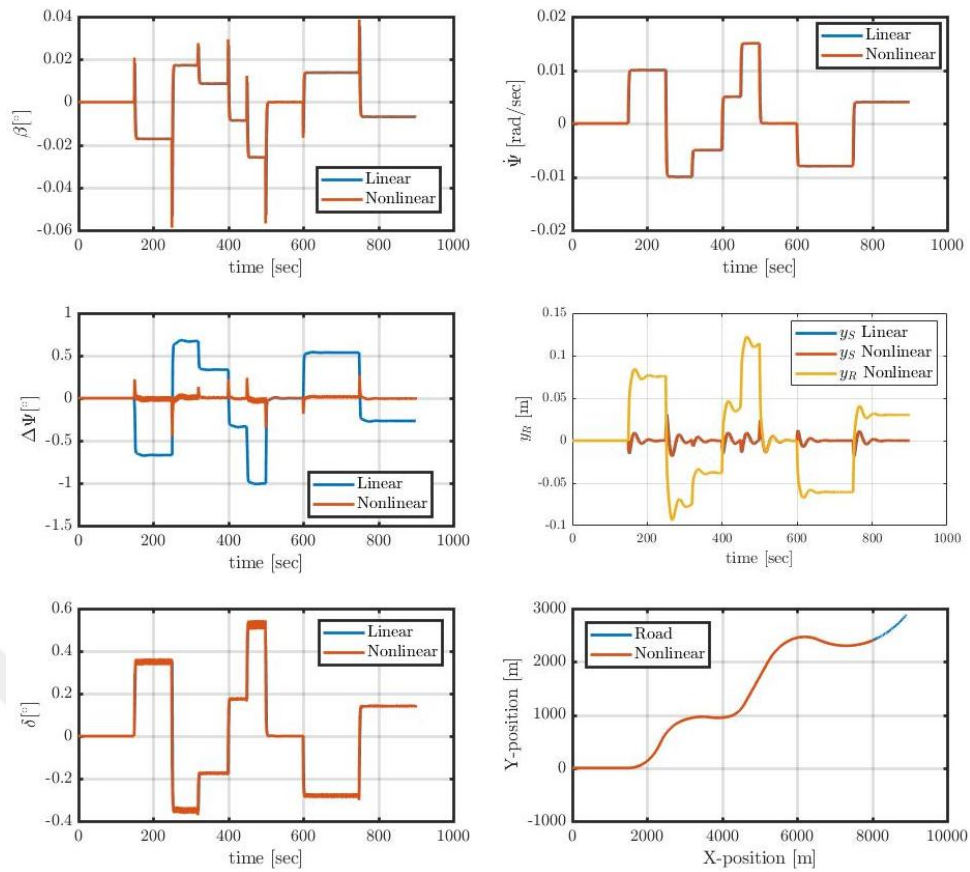


Figure 3.23: Nested PID control on the test road: $v=10$ m/s; $l_s = 12$ m (bus parameters)

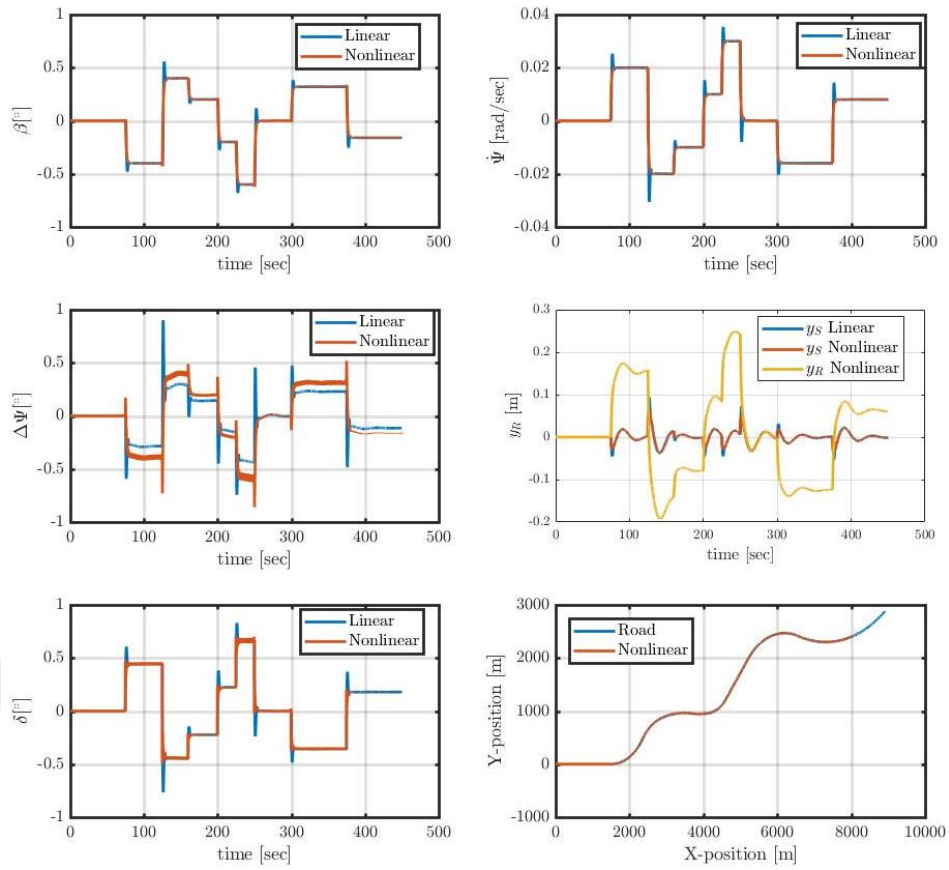


Figure 3.24: Nested PID control on the test road: $v=20$ m/s; $l_S = 12$ m (bus parameters)

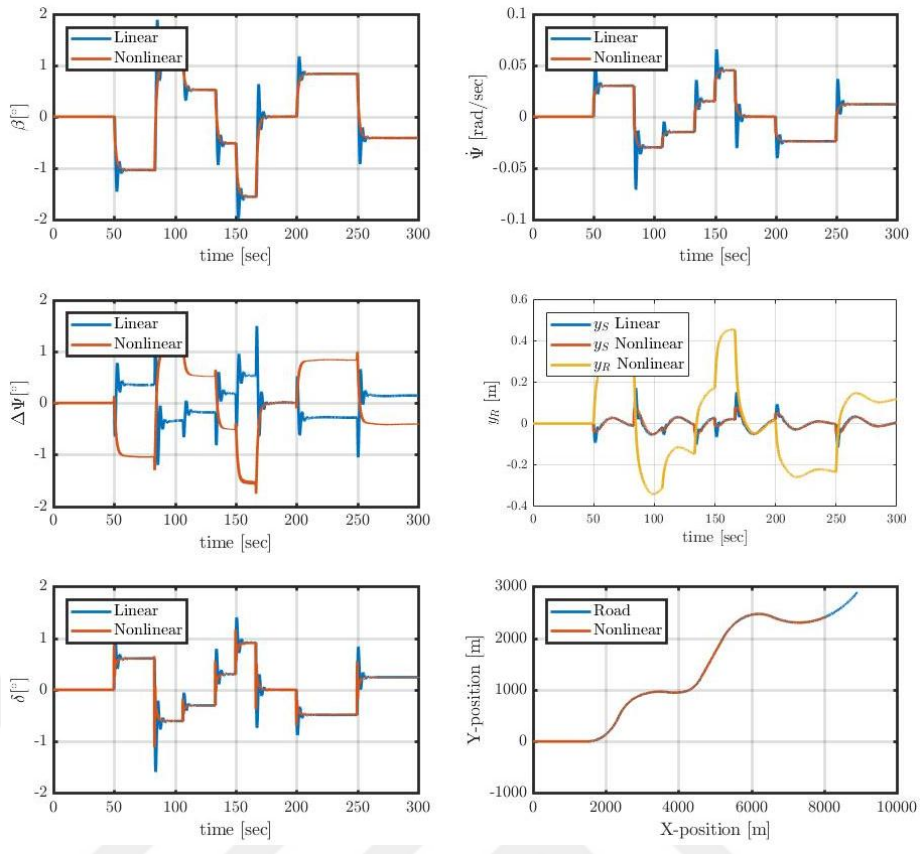


Figure 3.25: Nested PID control on the test road: $v=30$ m/s; $l_S = 12$ m (bus parameters)

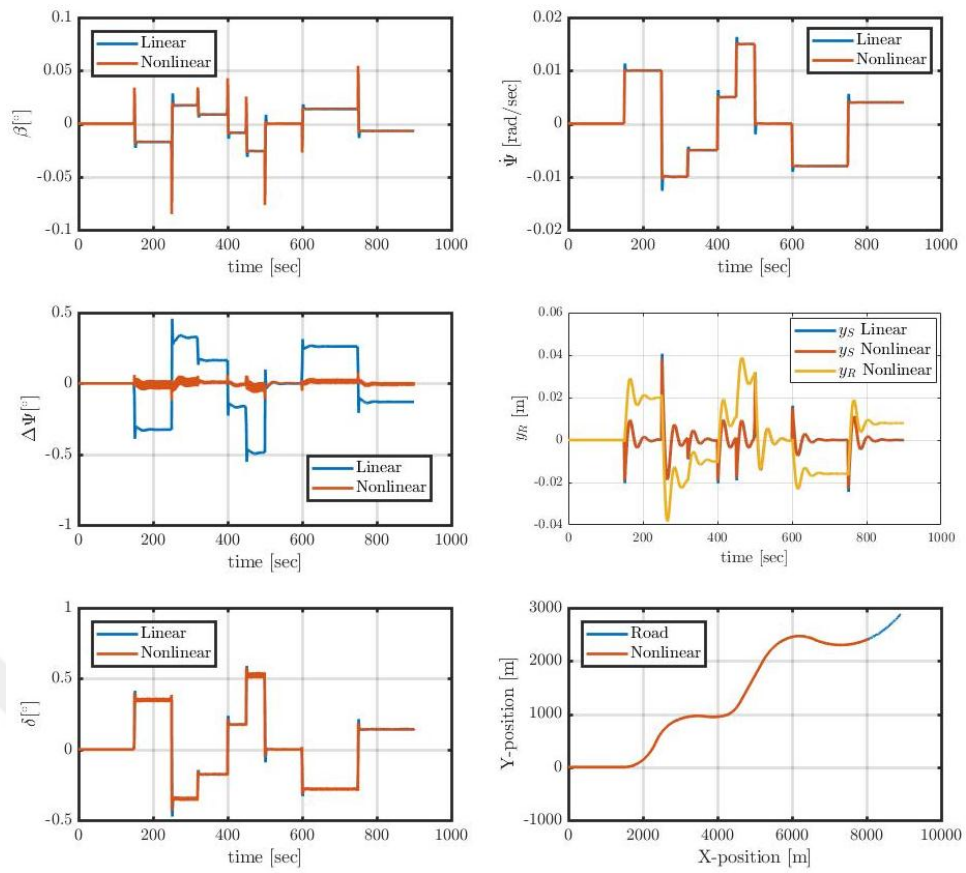


Figure 3.26: Nested PID control on the test road: $v=10$ m/s; $l_S = 6$ m (bus parameters)

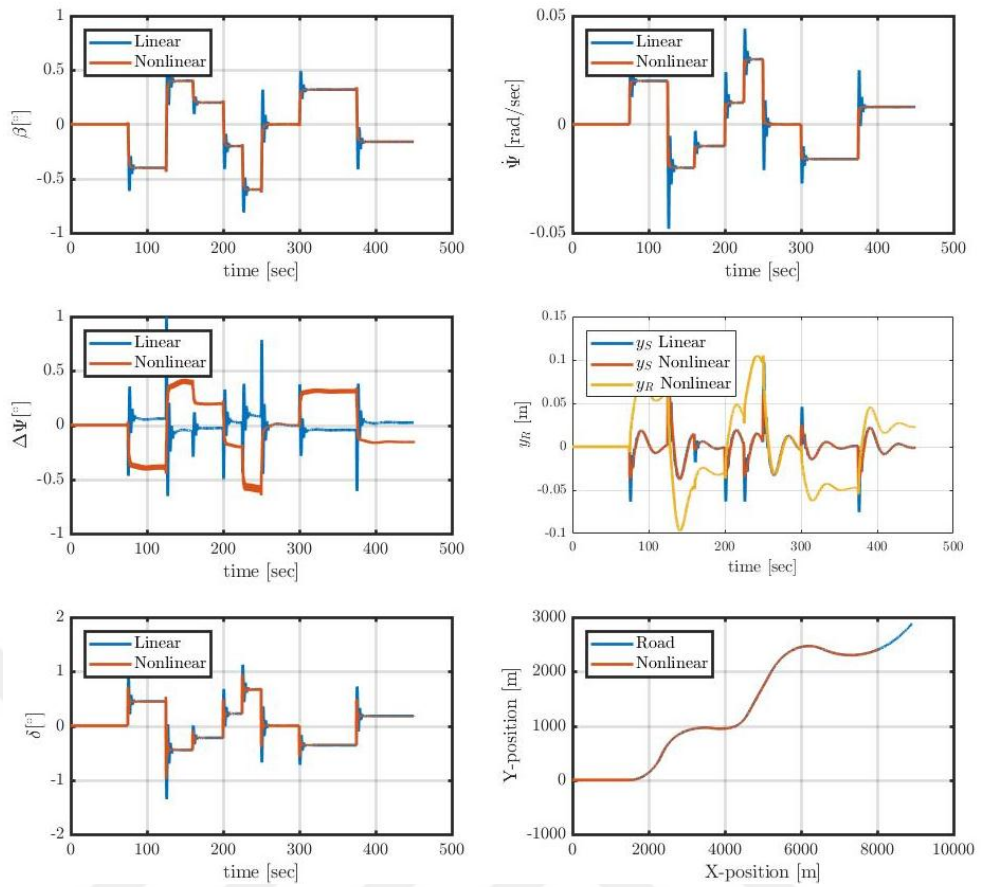


Figure 3.27: Nested PID control on the test road: $v=20$ m/s; $l_S = 6$ m (bus parameters)

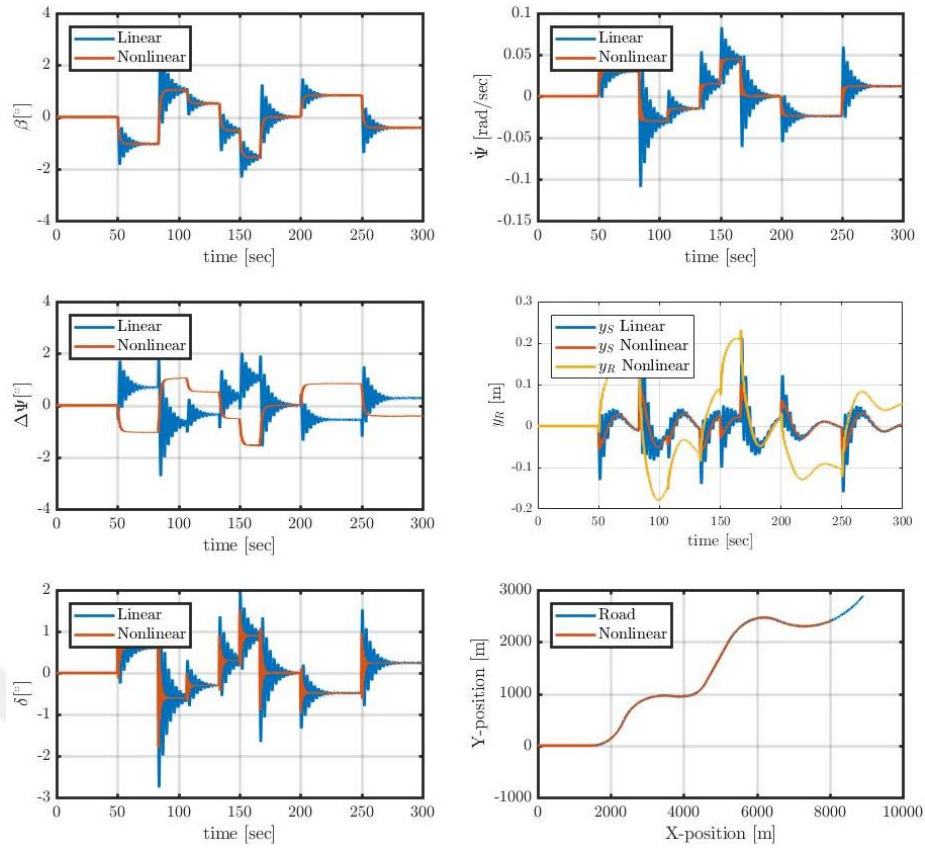


Figure 3.28: Nested PID control on the test road: $v=30$ m/s; $l_s = 6$ m (bus parameters)

3.4.3 Evaluation for Car Parameters

We first perform a simulation of for the car parameters with an initial displacement error of 1 m. Fig. 3.29 shows a fast convergence of the COG to the road center within less than 3 s. No overshoot is observed in this case.

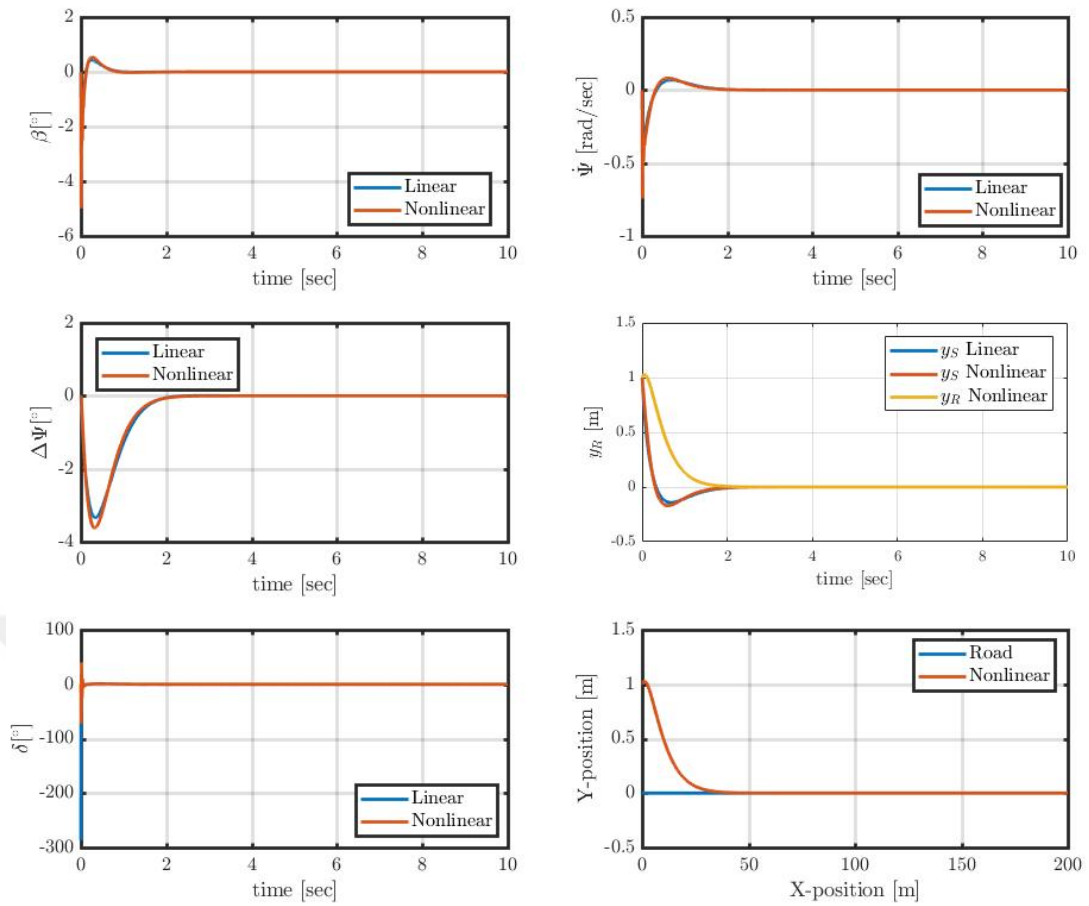


Figure 3.29: Nested PID: Response for an initial displacement error of 1 m (car parameters)

Fig. 3.30 also shows that the nested PID control is able to achieve small displacement errors for high speeds and small pre-view distances. That is, the nested PID control is suitable both for heavy vehicles and light vehicles.

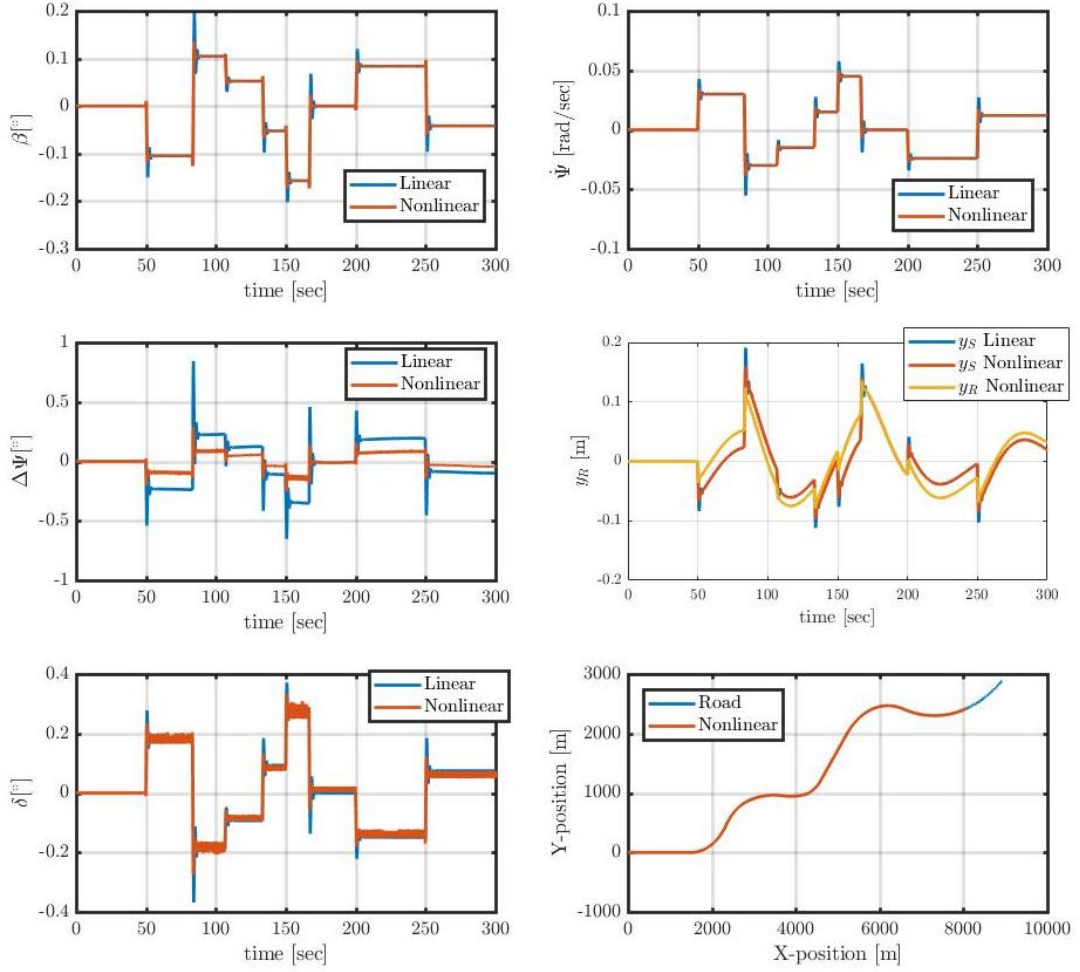


Figure 3.30: Nested PID control on the test road: $v=30$ m/s; $l_s = 6$ m (car parameters)

3.5 Empirical Controller

3.5.1 Description

The feedback loops and controllers in Section 3.2 to 3.4 are based on the linear model of the vehicle. The controller considered in this section is based on measurements of human driver behavior and is hence denoted as empirical controller [56].

This controller is based on measurements of the road curvature ρ , the displacement error y_R , the yaw rate $r = \dot{\psi}$ and the heading error $\Delta\psi$. It computed the rate of change of the steering angle as

$$\dot{\delta} = k \cdot \left(\frac{l_s}{2} \cdot \rho - \left(\frac{1}{l_s} \cdot y_R - \frac{l_s}{2 \cdot v} \cdot r + \Delta\psi \right) \right) \quad (3.13)$$

As a further simplification (3.13) can be integrated to directly compute the steering

angle

$$\delta = -\frac{k}{v} \cdot \left(y_R + \frac{v}{l_S} \int y_R + \frac{l_S}{2} \cdot \Delta\Psi \right) \quad (3.14)$$

The interesting fact is that this controller is a nonlinear controller since it is speed-dependent. To be precise, the controller in (3.14) is a PI type controller with gains that change with the speed. In addition, the part $y_R + \frac{l_S}{2} \cdot \Delta\Psi$ provides a lookahead distance.

The controller parameters chosen in this thesis are $k = 5$ and $l_S = 8$ m.

3.5.2 Evaluation for the Bus Parameters

We first consider an initial displacement of 1 m. The simulation results in Fig. 3.31 show that the response oscillates and it takes a long time until the vehicle converges to the road center. That is, the empirical controller cannot deal well with displacement errors.

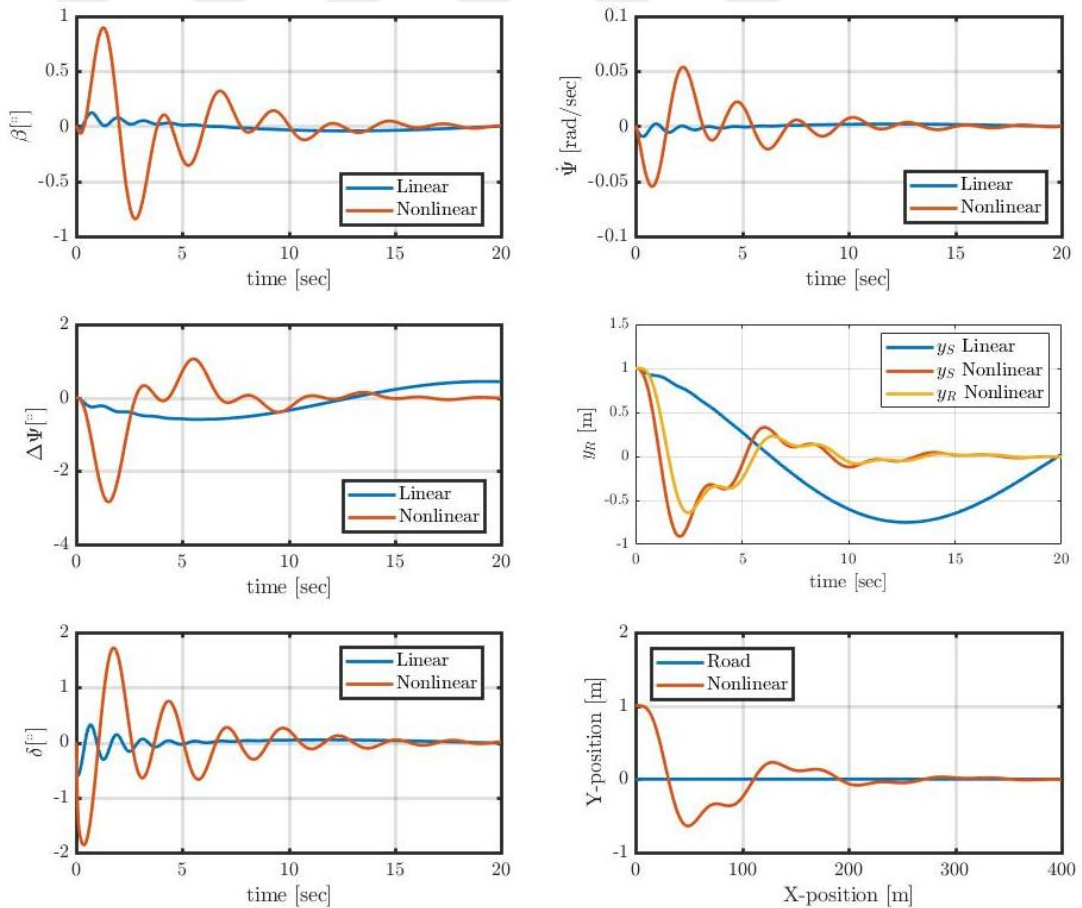


Figure 3.31: Empirical Control: Initial displacement error of 1 m (bus parameters)

A similar effect is observed in road tests. In all cases, oscillations are observed. The controller only ensures small displacement errors for small speeds of 10 m/s. In

addition, it is interesting to note that this controller does not perform well for the linear model, since it was not designed based on the linear model.

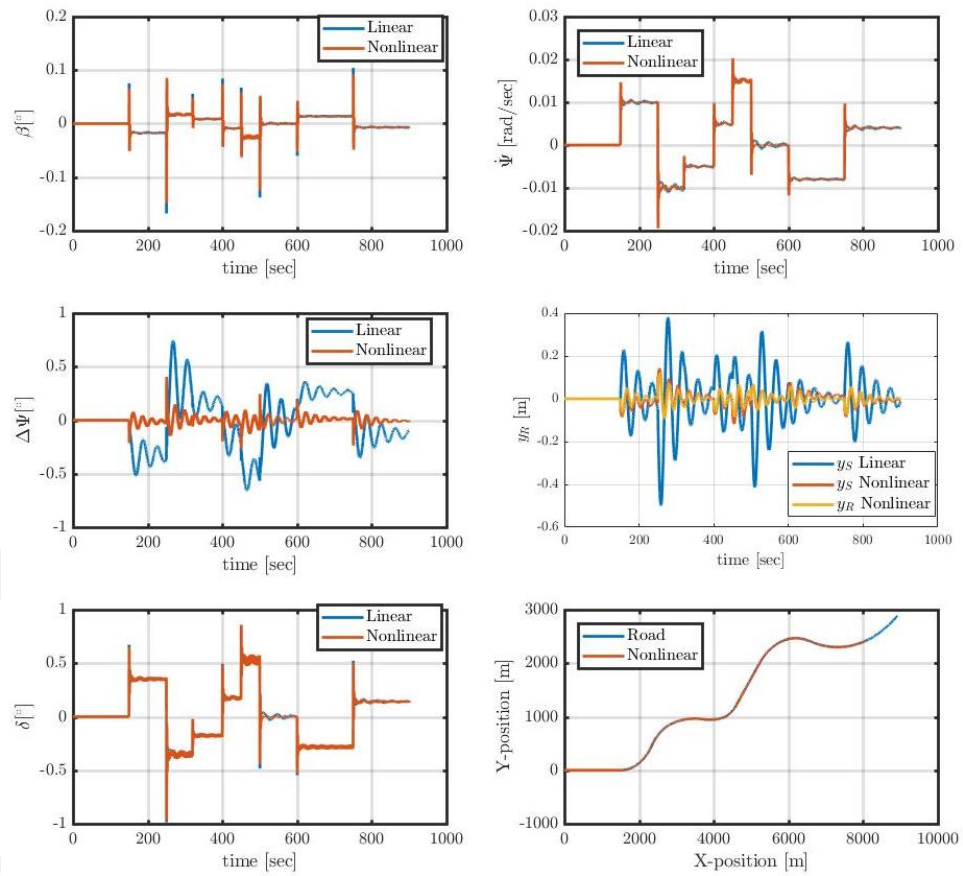


Figure 3.32: Empirical control on the test road: $v=10$ m/s (bus parameters)

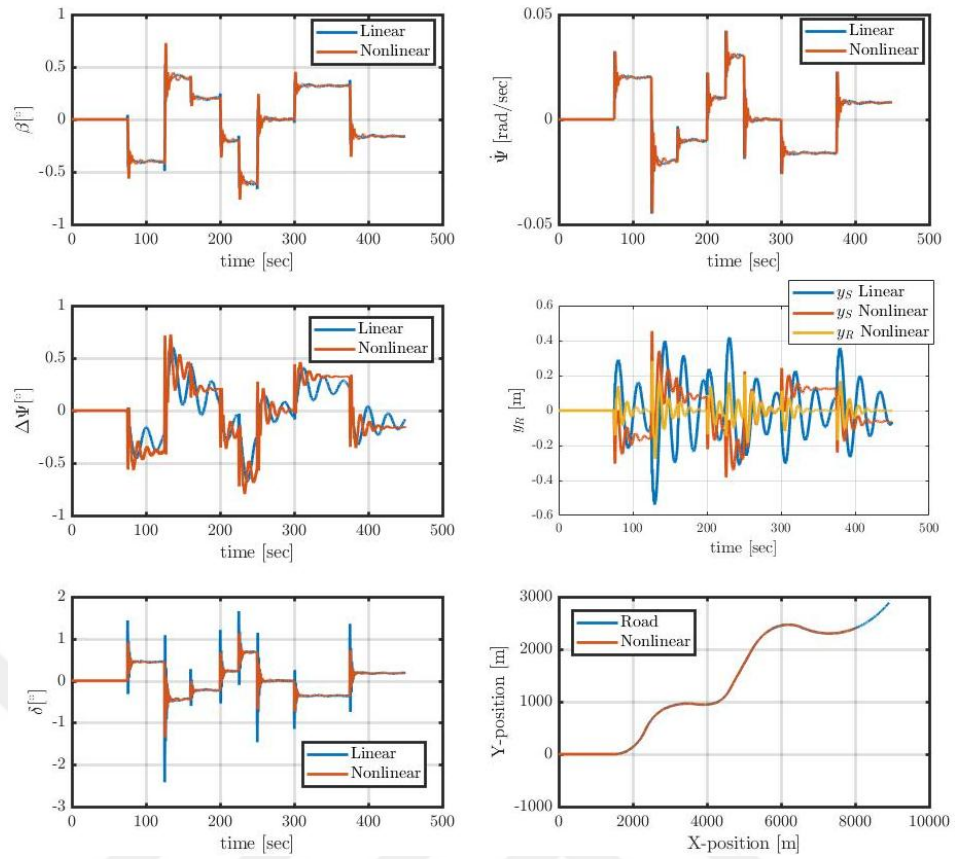


Figure 3.33: Empirical control on the test road: $v=20$ m/s (bus parameters)

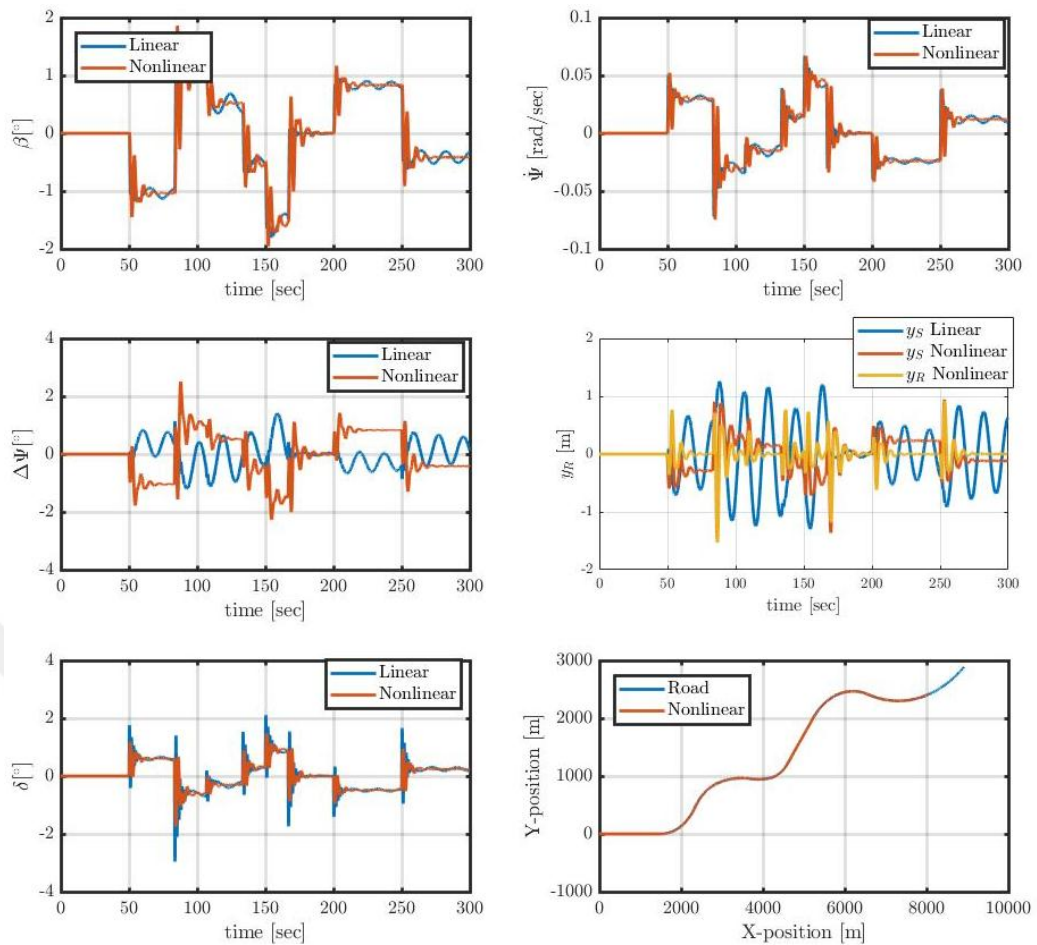


Figure 3.34: Empirical control on the test road: $v=30$ m/s (bus parameters)

3.5.3 Evaluation for the Car Parameters

The simulation results for the car parameters are very similar to the results shown for the bus parameters in Section 3.5.1. As an example, we only show the case of road following with $v = 20$ m/s. The responses show large oscillations and it could not be confirmed that the controller is suitable for lane keeping.

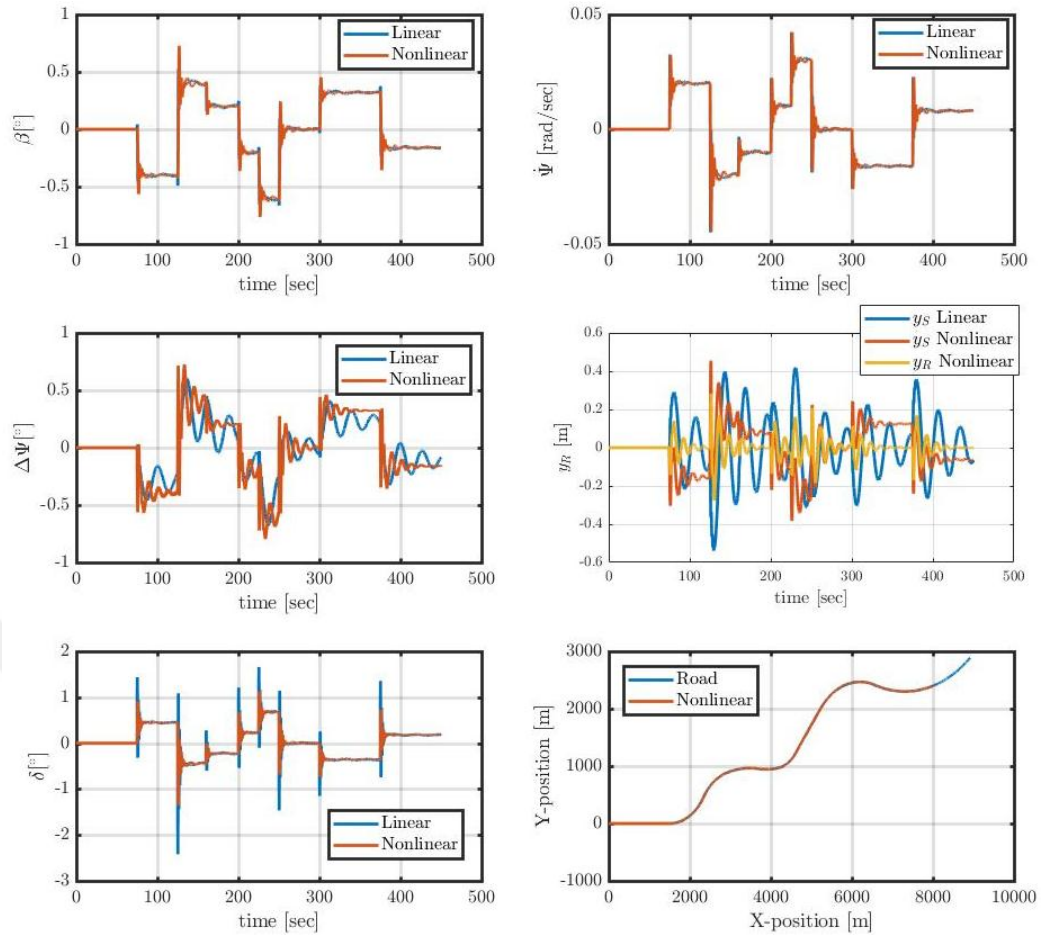


Figure 3.35: Empirical control on the test road: $v=20$ m/s (car parameters)

3.6 Suggested Controller

It can be seen from the previous experiments that the existing lane keeping control methods in Section 3.2 to 3.4 control the displacement error y_S at the pre-view distance l_S . As a result, the signal y_S remains small but the displacement error y_R at the COG can assume large values, which is undesired. On the other hand, it is also seen from the discussion in Section 3.5 that directly controlling y_R leads to oscillations and hence decreases the robustness of the lane keeping systems.

In this section, a new lane keeping control algorithm is suggested based on the nested PID control algorithm in Section 3.4. The same controllers are used. The only modification of Fig. 3.21 is that, instead of using the feedback signal y_S , the signal $y_S + y_R$ is used, which combines the displacement errors at the pre-view distance and at the COG. The next simulation experiments evaluate the modified control algorithm.

Fig. 3.34 shows the simulation result for an initial displacement of 1 m. It can be

seen that the vehicle position converges to the road center within less than 3 s and without overshoot.

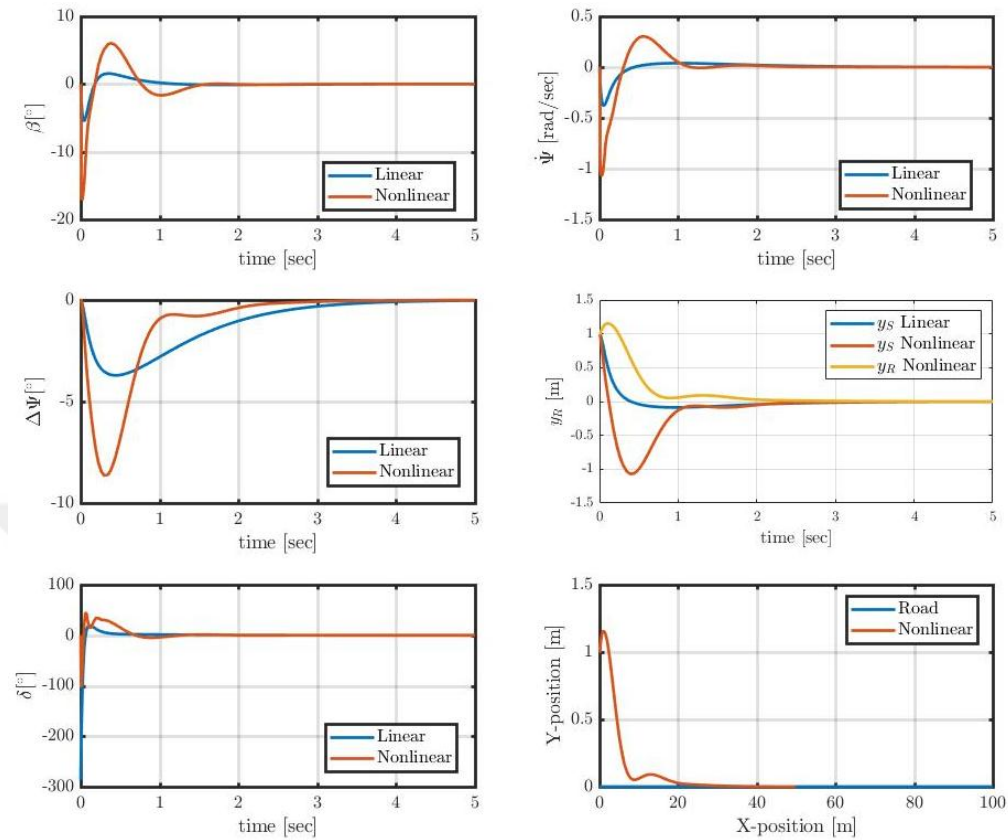


Figure 3.36: Proposed Control: Initial displacement error of 1 m (bus parameters)

Further simulation experiments on the test road are shown in Fig. 3.35 to 3.37. Here, the pre-view distance is chosen as $l_S = 12$ m and the speeds are $v = 10, 20, 30$ m/s. It can be seen from all the figures that choosing the feedback signal $y_S + y_R$ has an interesting effect. The displacement errors at the pre-view distance and at the COG are of similar size such that y_R is considerably reduced compared to the other control methods. At the same time, robustness of the feedback loop is preserved and there are no large oscillations. That is, choosing the proposed feedback signal improves the performance of the feedback loop. This fact is further illustrated in Section 3.7.

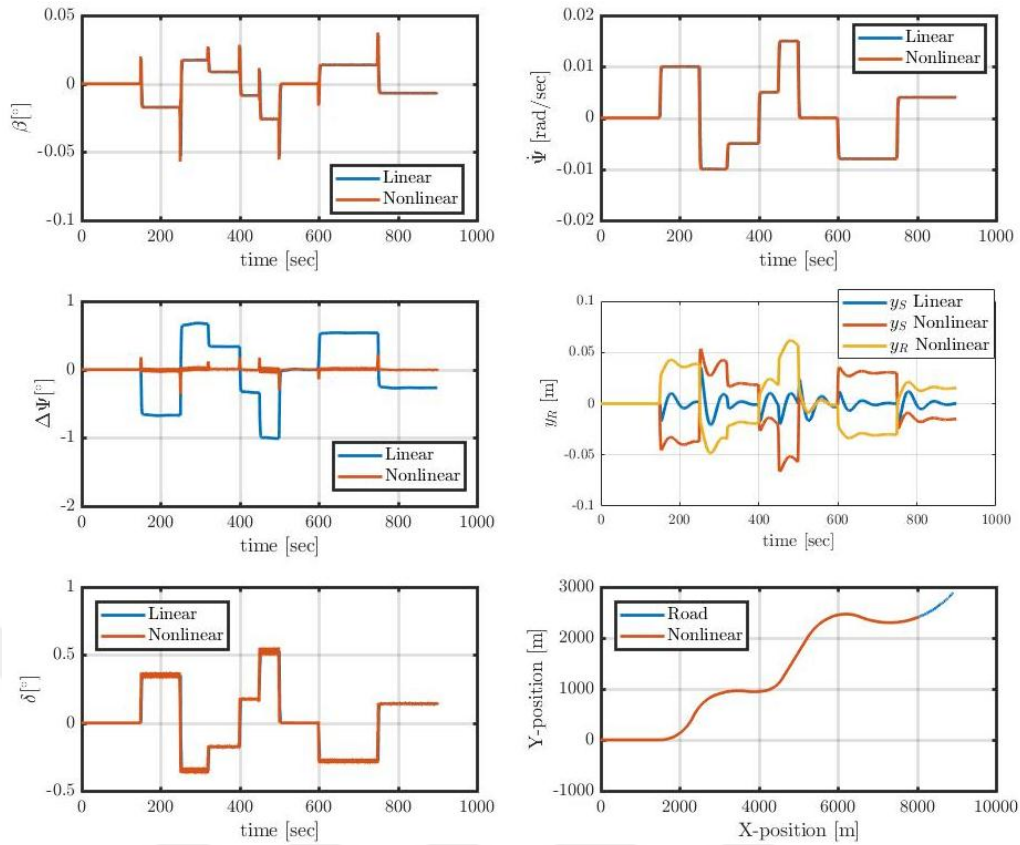


Figure 3.37: Proposed control on the test road: $v=10$ m/s (bus parameters)

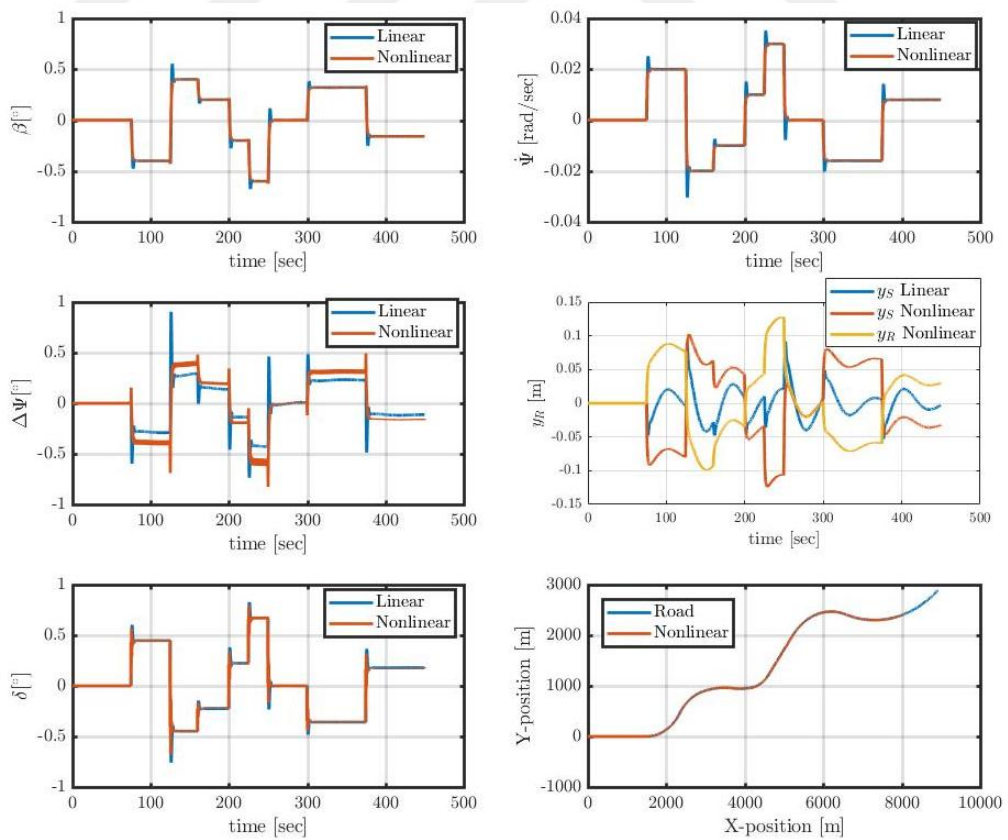


Figure 3.38: Proposed control on the test road: $v=20$ m/s (bus parameters)

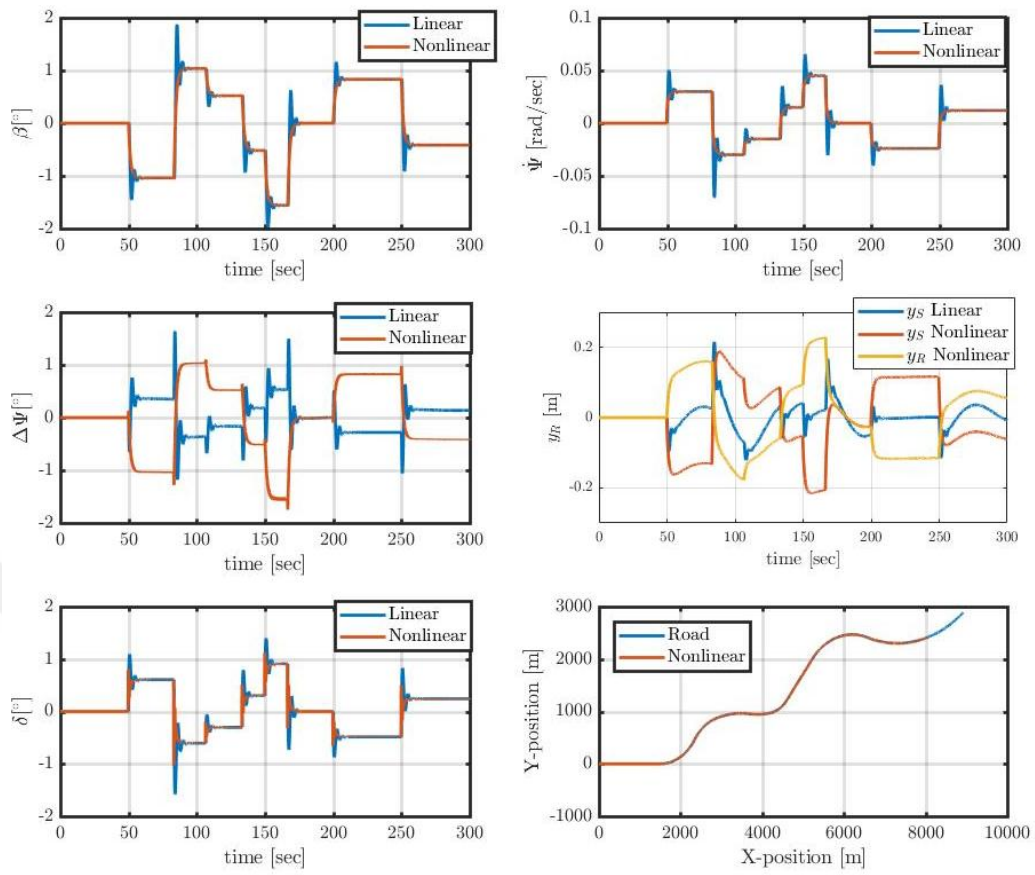


Figure 3.39: Proposed control on the test road: $v=30$ m/s (bus parameters)

3.7 Comparison of all Controllers

In this section, we perform a comparison of the different control algorithms presented so far. We first study the response to an initial displacement of 1 m. The resulting simulation is shown in Fig. 3.38. It can be seen that the sliding mode control and empirical control approaches show the slowest convergence to the road center. Additionally, the empirical control approach leads to large oscillations. The remaining methods all ensure a fast convergence to the road center.

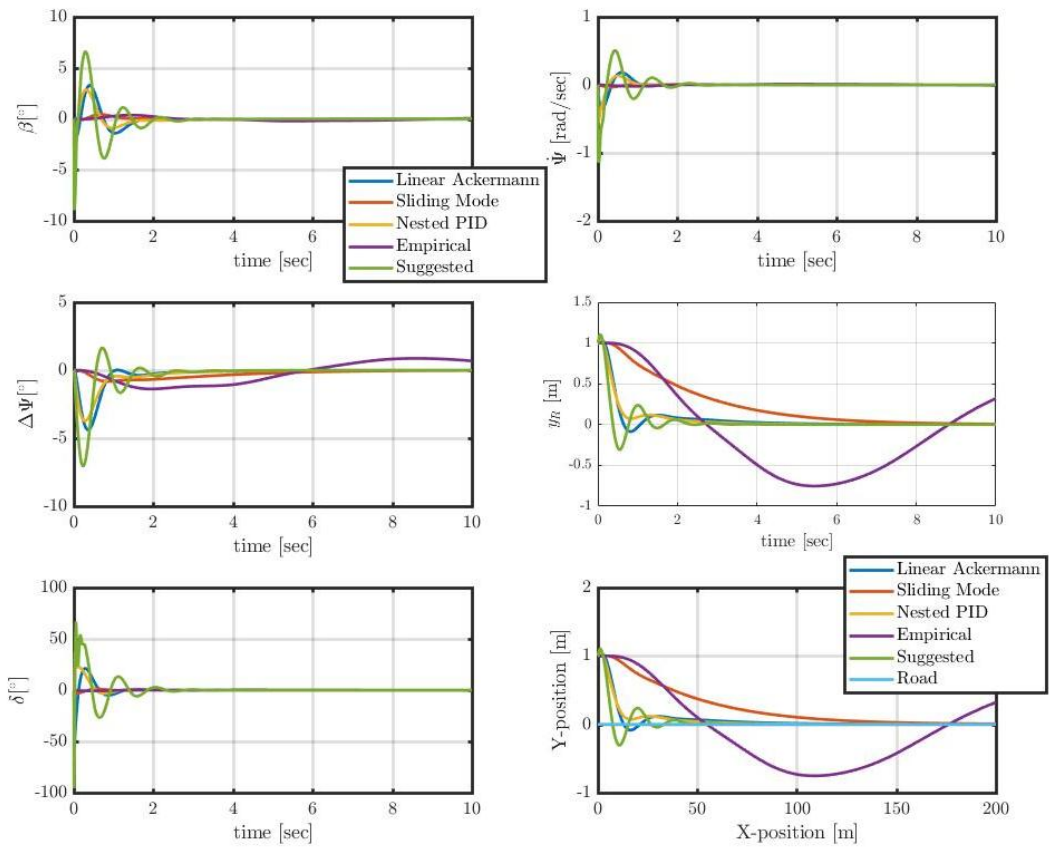


Figure 3.40: Controller Comparison: Initial displacement error of 1 m (bus parameters)

We further conduct experiments on the test road for different speeds in Fig. 3.39 to 3.41. The pre-view distance is chosen as $l_s = 12$ m. It can be seen from the figures that the empirical control approach leads to the largest displacement errors with oscillations. The smallest displacement error is achieved with the newly proposed method in Section 3.6. Similar conclusions can be drawn from Fig. 3.40 and 3.41 for higher speeds. In particular, the displacement error of the COG is reduced by around 50 % compared to the existing methods and remains below 0.2 m even at high speeds of 30 m/s.

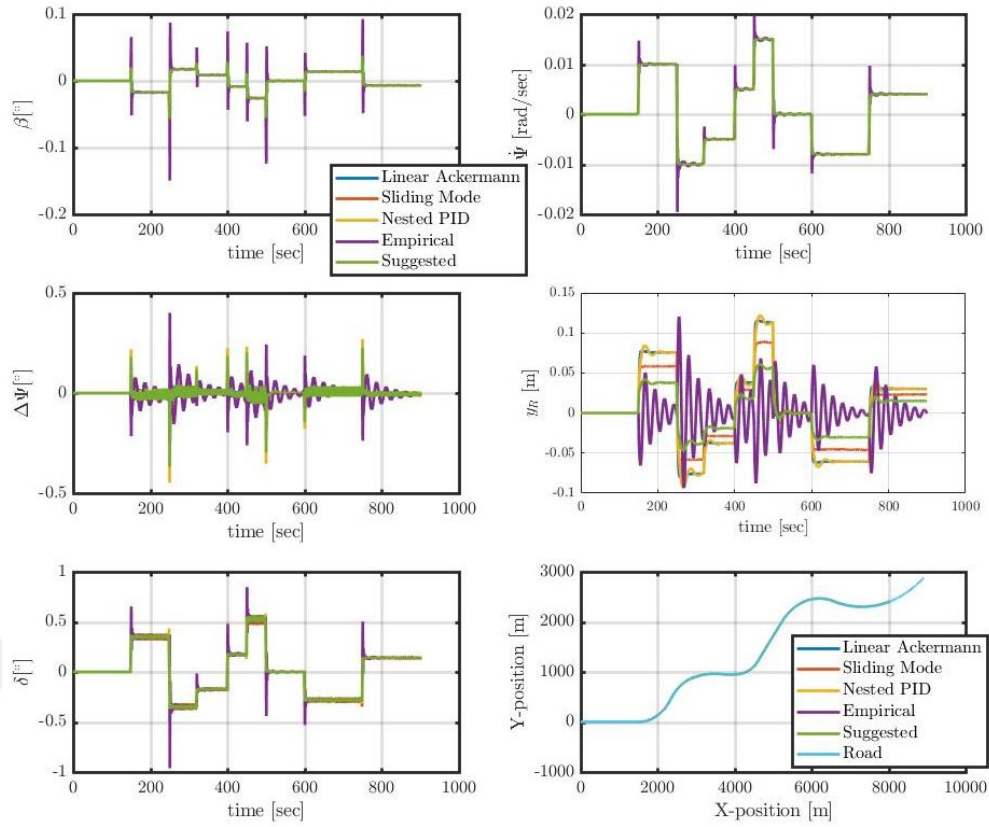


Figure 3.41: Controller Comparison on the test road: $v=10$ m/s (bus parameters)

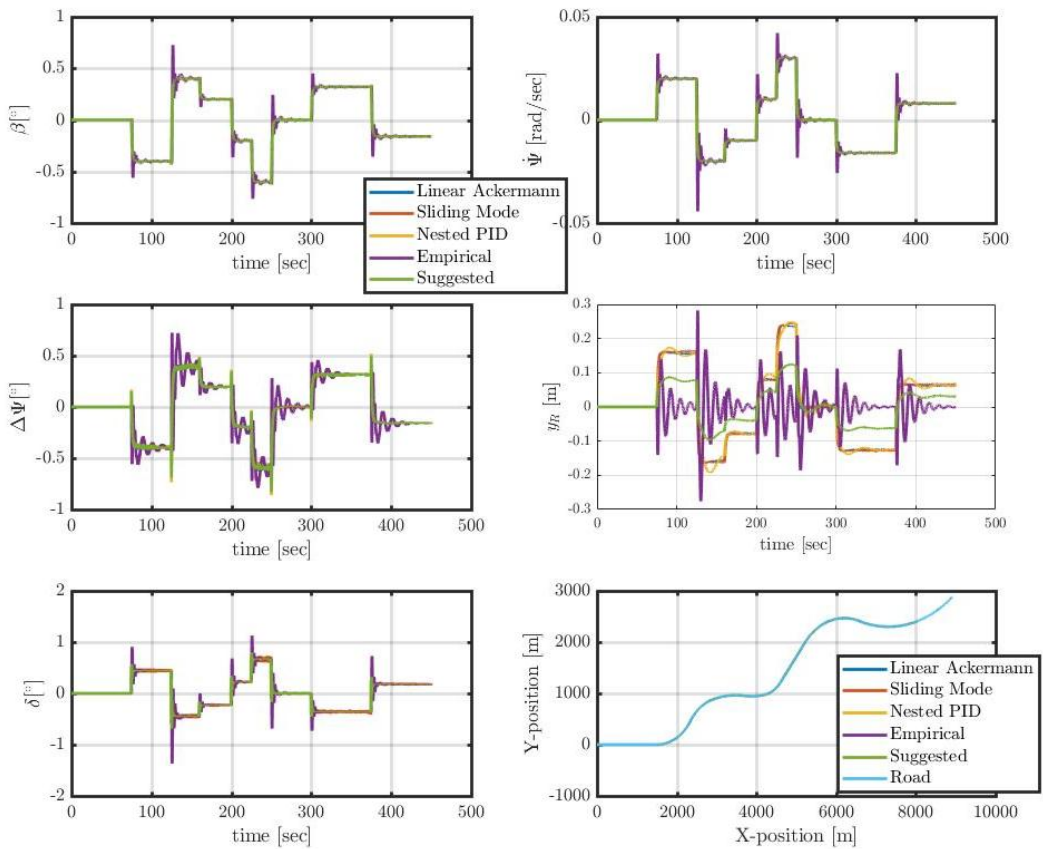


Figure 3.42: Controller Comparison on the test road: $v=20$ m/s (bus parameters)

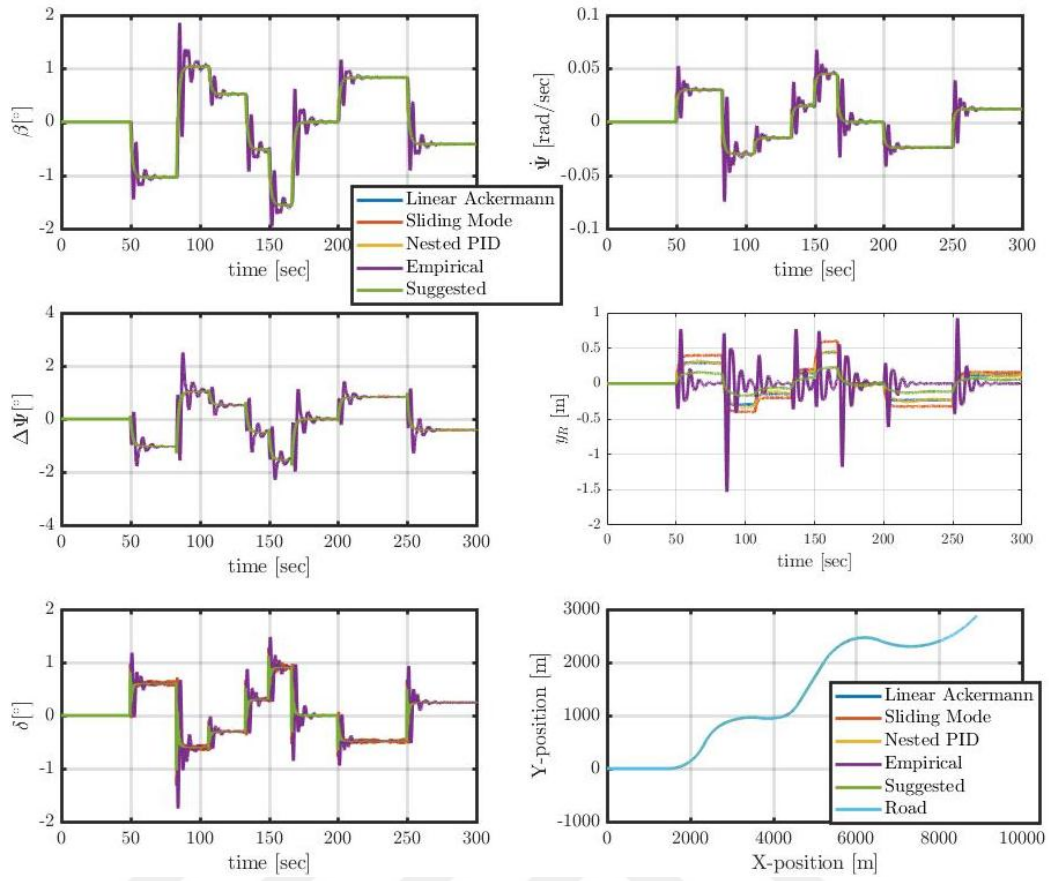


Figure 3.43: Controller Comparison on the test road: $v=30$ m/s (bus parameters)

CHAPTER 4

CONCLUSION

There is a recent interest in intelligent transportation systems both in industry and in the academic literature. One highly relevant application is lane keeping which automates the lateral motion of vehicles on the road to prevent traffic accidents and increase the comfort of drivers. Different sensors are required for the realization of lane keeping system including sensors for road detection and displacement error, velocity, yaw rate, heading error and the front steering angle. Using these sensors, the literature provides different control algorithms for lane keeping using different controller design methods.

In the presented thesis, linear and nonlinear control concepts for lane keeping on straight and curved roads were studied. First, a nonlinear vehicle model and its linearization were developed and implemented in Matlab/Simulink. Then, four different control algorithms from the existing literature were realized and compared in a simulation study. It was shown that most of the existing algorithms have a particular disadvantage that was not identified before. Since the algorithms control the displacement error of the vehicle at a given pre-view distance, it turns out that the actual vehicle displacement can assume unnecessarily large values on curved roads. Only one algorithm directly controls the vehicle displacement. However, this algorithm has the disadvantage of large oscillations around the road center which are undesired. As a remedy, the thesis further proposes a new lane keeping control method that combines measurements of the actual vehicle displacement (for precision) and the vehicle displacement at a pre-view distance (for robustness). The comparative simulation study in the thesis shows that the proposed method has superior performance compared to the existing methods.

REFERENCES

- [1] **LEE, J. H.** (2008) Fifty Years of Driving Research, *Human Factors*, 521-528. Vol. 50.
- [2] **YOUNG, M. S.** (1998) Vehicle Automation and Driving Performance, *Ergonomics*, 1014-1028. Vol. 41(7).
- [3] **WALKER, G. H., STANTON, N.A., YOUNG, M. S.** (2009) Where is Computing Driving Cars ? , *International Journal of Human Computer Interaction*, 203-229. Vol. 13(2).
- [4] **SHLADOVER, S.** (1995) Review of The State of Development of Advanced Vehicle Control Systems (AVCS), *Vehicle System Dynamics*, 551-592. Vol.24(6).
- [5] **TEFFT, B. C.** (2012) Prevalence of Motor Vehicle Crashes Involving Drowsy Drivers, United States, 1999-2008, *Accident Analysis & Prevention*, 180-186. Vol. 45.
- [6] **ZADOR, P.L., KRAWCHUK, S.A., , and VOAS, R.B.** (2000) *Automotive Collision Avoidance System (ACAS) Program.*, Final Report DOT HS 809 080, DOT/NHTSA, Washington, DC,USA, August. Available at: http://www-rd.nhtsa.dot.gov/departments/nrd-12/pubs_rev.html
- [7] **GOLIAS, J., YANNIS, G., and ANTONIOU, C.** (2002) Classification of Driver-Assistance Systems According to Their Impact on Road Safety and Traffic Efficiency, *Transport Reviews*, 179-196, Vol.22.
- [8] **JAGTMAN, M., MARCHAU, V.A.W.J., and HEIJER, T.** (2001) *Current Knowledge on Safety Impacts of Collision Avoidance Systems (CAS).* In P.M. Herder and W.A.H. Thissen, editors, Proceedings of the 5th International Conference on Technology, Policy and Innovation, Delft, June 26–29.
- [9] **TREAT, J.R.** (1980) A study of Precrash Factors Involved in Traffic Accidents. *HSRI Research Review*, 1–35. Vol.10.
- [10] **BOSE, A., and IOANNOU, P. A.** (2001) *Analysis of Traffic Flow with Mixed Manual and Intelligent Cruise Control (ICC) vehicles: Theory and experiments*, UCB-ITS-PRR-2001-13, California PATH, Berkeley, CA, USA, April. Available at: <http://www.path.berkeley.edu/PATH/Publications/PDF/PRR/2001/PRR-2001-13.pdf>
- [11] **IOANNOU P.A. and STEFANOVIC M.** (2005) Evaluation of ACC Vehicles in Mixed Traffic: Lane Change Effects and Sensitivity analysis. *IEEE Transactions on Intelligent Transportation Systems*, 79–89. Vol. 6.

- [12] **ZWANEVELD, P. and van AREM, B.** (1998) Traffic Effects of Automated Vehicle Guidance Systems. In Proceedings of the 5th World Congress on Intelligent Transport Systems (ITS), Seoul, Korea, October 12–16.
- [13] **LIU, J. F., Hu, T. H., HSU, T. H.** (2001) Design of an Automative Lane Keeping System Based on the Structure of Electric Power Steering, *International Journal of Vehicle Mechanics and Mobility*, 391-411. Vol.36.
- [14] **PARASURAMAN, R., RILEY, V.** (1997) Humans and Automation :Use , Misuse, Disuse, Abuse, *Human Factors*, 230-253. Vol.39.
- [15] **PARSURMAN, R., MANZEY, D. H.** (2010) Complacency and Bias in Human Use of Automation: An Attentional Integration , *Human Factors* , 381-410. Vol. 52.
- [16] **SARTER, N.B., WOODS, D.D.** (1995) How in the world did we ever get into that mode? Mode error and awereness in supervisory control, *Human Factors*, 5-19. Vol.37.
- [17] **MAMMAR, S.** (1997) *Robust Automatic Steering of a Vehicle: An LMI Approach*, IFAC Transportation Systems, Chania, Greece, 371-376.
- [18] **MAMMAR, S.** (1998) *Robust Automatic Steering Using Fuzzy Modelling and LMI Control*, IFAC System Structure and Control, Nantes, France, 503-508.
- [19] **HATIPOĞLU, C., ÖZBAY, H., ÖZGÜNER, Ü., ŞAHİN, B.** (1998) H_{∞} Controller Design for Automatic Steering of Vehicles With Modeled Time Delays, Proceedings of the IEEE Conference on Intelligent Transportation Systems, Boston MA, November, 260-265.
- [20] **HATIPOGLU, C., REDMILL, K., OZGUNER, U.** (1998) *Automated Lane Change: Theory and Practice*, In Preprints of the IFAC Workshop on Advances in Automotive Control, Mohican State Park, Ohio, February, 73-78.
- [21] **RAKSINCHAROENSK, P., MOURI, H., NAGAI, M.** (2002) *Lane Tracking Control Performance of Four Wheel –Steering Automobile*, Proceedings of IFAC 15th Triennial World Congress, Barcelona, Spain, 385-390.
- [22] **RAHARIJAONA, T., DUC, G., MAMMAR, S.** (2004) *H_{∞} controller synthesis and analysis with application to lateral driving assistance*, Proceedings of IFAC Advances in Automative Control, Selerno, Italy, 637-642.
- [23] **YOU, S. S., JEONG, S. K.** (2004) Automatic Steering Controllers for General Lane-Following Manoeuvres of Passanger Cars using 2-DOF Robust Control Synthesis, *Transactions of the Institute of Measurement and Control*, 273-292. Vol.26
- [24] **ZAMBOU, N., BOLLIG, A., ABEL. D., SIEDERSBERGER, K. H., MÜLLER, K.** (2005) *Application of Model-Based Predictive and Robust Loop Shaping Control To Automatic Car Steering*, Proceedings of IFAC 16th Triennial

World Congress, Prague, Czech Republic, 85-90.

[25] **JUNG, C.R., KELBER, C.R.** (2005) Lane Following and Lane Departure using a linear-parabolic model, *Image and Vision Computing*, 1192-1202. Vol.23.

[26] **WANG, Q., OYA, M., KOBAYASHI, T.** (2006) *Adaptive Steering Control Scheme for Combination Vehicles To Track Target Lane*, Proceedings of SICE-ICASE International Joint Conference, Busan, Korea, 1790-1795.

[27] **KOUMBOULIS F. N., SKARPETIS, M. G. and PANAGIOTAKIS ,G. E.** (2006) Robust Disturbance Rejection via P-D State Feedback – Example for Lane Keeping of Highway Vehicles, *Transactions of the Institute of Measurement & Control*, 141-143. Vol. 28.

[28] **CERONE, V., MILANESE, M., REGRUTO, D.** (2007) *Simulation Results on Combined Automatic Lane Keeping and Driver's Maneuvers*, Proceedings of European Control Conference, Kos, Greece, 1241-1248.

[29] **GUNAY, B.** (2008) A Methodology on the Automatic Recognition of Poor Lane Keeping, *Journal of Advanced Transportations*, 129-149. Vol. 42.

[30] **ZHANG J., REN, D.** (2009) *Lateral Control of Vehicle for Lane Keeping in Intelligent Transportation Systems* , Proceedings of International Conference on Intelligent Human- Machine Systems and Cybernetics, Zhejiang, Chiana ,446-450.

[31] **CERONE, V., MILANASE, M.,REGRUTO, D.** (2009) Combined Automatic Lane –Keeping and Maneuvers Trough A 2-DOF Control Strategy , *IEEE Transactions on Control Systems Technology*,135-142, Vol.17.

[32] **WANG, J., LIN, C., CHEN, S.** (2010) Applying Fuzzy Method to Vision Based Lane Detection and Departure Warning System, *Expert Systems with Applications*, 113-126. Vol. 37.

[33] **ZHAO, J., LEFRANC, G., EL KAMEL, A.** (2010) Lateral Control of Autonomous Vehicles Using Multi-Model and Fuzzy Approaches, *IFAC Proceedings*, ,514-520, Vol.43.

[34] **MARINI. R., SCALZI, S., NETTO, M.** (2011) Nested PID Steering for Lane Keeping in Autonomous Vehicles, *Control Engineering Practice*, 1459-1467., Vol. 19.

[35] **PING, E. P., SWEE, S.K.** (2012) *Simulation and Experiment of Automatic Steering Control for Lane Keeping Manoeuvre* , Proceedings of 4th International Conference on Intelligent and Advanced Systems, Kuala Lumpur, Malaysia, 105-110.

[36] **DOI, M., ZENG, K.,WADA, T., DOI, S., TSURU, N., ISAJI, K.** (2013) *Steering-Assist Control Systems on Curved Road Using Car-to-car Communication*, Proceedings of the 16th International IEEE Annual Conference , The Hague, The

Netherlands, 6-9.

[37] **MASHADI, B., MAHMOUDI, M., KAKAEE, A., HOSSEINI, R.** (2013) Vehicle Path Following Control In the Presence of Driver Inputs, *Journal of Multi-body Dynamics* , 115-132. Vol.227.

[38] **RUCCO. A., NOTARSTEFANO, G., HAUSER, J.** (2014) Optimal Control Based Dynamics exploration of a Rigid Car With Longitudinal Load Transfer, *IEEE Transactions on Control Systems Technology*, 1070-1077. Vol.22.

[39] **CHEN, B., LUAN, B., LEE, K.** (2014) *Design of Lane Keeping System Using Adaptive Model Predictive Control*, Proceedings of the IEEE International Conference on Automation Science and Engineering, Taipei, Taiwan, 18-22.

[40] **WILLIAMS, D.E.** (2014) Lane-keeping benefits of practical rear axle steer, *Vehicle System Dynamics*, 504-521. Vol.52.

[41] **SON, Y., KIM, W., LEE, S., CHUNG C.** (2015) Robust Multirate Control Scheme With Predictive Virtual Lanes for Lane-keeping Systems of Autonomous Highway Driving, *IEEE Transactions on Vehicular Technology*, 3378-3391. Vol.64.

[42] **LEI, J.** (2016) Research on a kind of sliding mode lane keeping control for automated vehicles based on hybrid information of position and angular velocity, *Optik*, 9344-9360. Vol.127.

[43] **MARTINEZ-GARCIA, M., ZHANG Y., GORDON, T.** (2016) Modelling Lane Keeping by a Hybrid Open-Closed-Loop Pulse Control Scheme, *IEEE Transactions on Industrial Informatics*, 2256-2264. Vol.12.

[44] **LEI, J., WU, H., YANG J., ZHAO, J.** (2016) Sliding Mode Lane Keeping Control Based on Sseparation of Translation and Rrotation Movement, *Optik*, 4369-4374. Vol.127.

[45] **KIM, W., SON, Y., CHUNG, C.** (2016) Torque-Overlay-Based Robust Steering Wheel Angle Control of Electrical Power Steering for a Lane –Keeping System of Automated Vehicles, *IEEE Transactions on Vehicular Technology*, 4379-4392. Vol.65.

[46] **SOLTANI, A., ASSADIAN, F.** (2016) A Hardware –in-the-Loop Facility for Integrated Vehicle Dynamics Control System Design and Validation, *IFAC-PapersOnline*, 032-038. Vol.49-21.

[47] **SCHMIDT, K. W.,** Vehicle Dynamics Models That are Suitable for Lane Change Computations, 1-9.

[48] **SCHMIDT, K. W., KAHYA, A.H. M. A.,** Optimal Control Methods for Lane Change Maneuvers, 1-20.

- [49] **KAHYA, A.H. M. A.** (2017) Optimal Control Problems for Safe and Efficient Lane Changes at Self Driving Vehicles.
- [50] **KAHYA, A.H. M. A., SCHMIDT, K. W.** (2016) Ensuring Spring Stability for Cooperative Adaptive Cruise Control on Curved Roads, *Journal of Vibration and Control*, 1-7.
- [51] **ACKERMANN, J., GULDNER, J., SINEL, W., STEINHAUSER, R., UTKIN, V.** (1995) Linear and Nonlinear Controller Design for Robust Automatic Steering, *IEEE Transactions on Control Systems Technology*, 132-143. Vol.3.,
- [52] **GULDNER, J., UTKIN, V., ACKERMANN, J.** (1994) *A Sliding Mode Control Approach to Automatic Car Steering*, Proceedings of the American Control Conference, Baltimore, Maryland, TPI-5:20.
- [52] **ACKERMANN, J., GULDNER, J., UTKIN, V.,** (1994) *A Robust Nonlinear Control Approach To Automatic Path Tracking of A Car*, Control '94 Conference Publications No.389.
- [54] **BAUMGARTEN, G** (2004) Motor vehicle steering system having a yaw rate controller, Bayerische Motoren Werke, United States Patent Pub.No.US20040070268
- [55] **GRASSI, E., TSAKALIS, K.S., DASH, S., Gaikwad, S.V., MacArthur, W & Stein, G.** (2001) Integrated system identification and PID controller tuning by frequency loop- shaping, *IEEE Transactions on Control Systems Technology*, 285–294. Vol. 9.
- [56] **TAN, H.S. , HUANG, J** (2014) Design of a High-Performance Automatic Steering Controller for Bus Revenue Service Based on How Drivers Steer, *IEEE Transactions on Robotics*, 1137-1147, Vol.30.
- [57] **KONG, J. , PHEIFFER, M. , SCHILDBACH, G. , BORELLI, F.** (2015) , *Kinematic and Dynamic Models for Autonomous Driving Control Design*, Proceedings of IEEE Intelligent Vehicles Symposium, Seoul, South Korea.
- [58] **POLACK, P., ALTICHE, A., ANDREA-NOVEL, B., LA FORTELLA, A.** (2017) *The Kinematic Bicycle Model : a Consistent Model for Planning Feasible Trajectories for Autonomous Vehicles*, Proceedings of IEEE Intelligent Vehicles Symposium (IV) , , Los Angeles, United States.
- [59] **RUCCO, A., NOTARSTEFANO, G., HAUSER, J.** (2014), Optimal Control Based Dynamics Exploration of a Rigid Car With Longitudinal Load Transfer, *IEEE Transactions on Control Systems Technology*, Vol.22.
- [60] **TAN, H.S. , GULDNER, J. , CHEN, C. , SATYAJIT, P. , BOUGLER, B.** (2000) Lane-changing with look-down reference systems on automated highways, *Control Engineering Practice*, 1033-1043. Vol.8.
- [61] **TURRI, V. , CARVALHO, A. , TSENG, H.E. , JOHANSSON, K.H. , BORELLI, F.** (2013) *Linear Model Predictive Control for Lane Keeping and*

Obstacle Avoidance on Low Curvature Roads, Proceedings of the 16th International IEEE Annual Conference on Intelligent Transportation Systems, The Hague, The Netherlands

[62] **ZHOU, S. , JIANG, Y., XI, J., GONG, J. , XIONG, G. , CHEN, H.** (2010), *A Novel Lane Detection based on Geometrical Model and Gabor Filter*, Proceedings of IEEE Intelligent Vehicles Symposium (IV), 59–64 .

[63] **WANG, Q. , OYA, M. , KOYABASHI, T.** (2006), *Adaptive Steering Control Scheme for Combination Vehicles to Track Target Lane*, Proceedings of SICE-ICASE International Joint Conference, Busan, Korea.

[64] **SENTOUH, C. , SOUALMI, B. , POPIEL J.C. , DEBERNARD, S.**(2013), *Cooperative Steering Assist Control System*, Proceedings of IEEE International Conference on Systems, Man and Cybernetics, Washington, DC, USA.



CURRICULUM VITAE

PERSONAL INFORMATION

Surname, Name: SARAÇOĞLU Kıvanç

Nationality: Turkish

Date and Place of Birth: 10/07/1991, Ankara, Turkey

Marital Status: Unmarried

Phone. +905056761055

E-mail: kivancsaracoglu@gmail.com

Hobbies: Playing Piano, Swimming, Reading, Electronic

EDUCATION

Degree	Institution	Year
B.Sc.	Çankaya University	2014
High School	Jale Tezer High School	2009